Developmental changes resemble stochastic optimization

Anna P. Giron[1,2,*], Simon Ciranka[3,4,*], Eric Schulz[5], Wouter van den Bos[6,7], Azzurra Ruggeri[8,9,10], Björn Meder[8,11], and Charley M. Wu[1,3,+]

[1]Human and Machine Cognition Lab, University of Tübingen, Tübingen, Germany
[2]Attention and Affect Lab, University of Tübingen, Tübingen, Germany
[3]Center for Adaptive Rationality, Max Planck Institute for Human Development, Berlin, Germany
[4]Max Planck UCL Centre for Computational Psychiatry and Ageing Research, Berlin, Germany
[5]MPRG Computational Principles of Intelligence, Max Planck Institute for Biological Cybernetics
[6]Department of Psychology, University of Amsterdam, Amsterdam, The Netherlands
[7]Amsterdam Brain and Cognition, University of Amsterdam, Amsterdam, The Netherlands
[8]MPRG iSearch, Max Planck Institute for Human Development, Berlin, Germany
[9]School of Education, Technical University Munich, Munich, Germany
[10]Central European University, Vienna, Austria
[11]Health and Medical University, Potsdam, Germany
[*]These authors contributed equally to this work
[+]Corresponding author: charley.wu@uni-tuebingen.de

ABSTRACT

Analogies to stochastic optimization are common in developmental psychology, describing a gradual reduction in randomness ("cooling off") over the lifespan. Yet for lack of concrete empirical comparison, there is ambiguity in interpreting this analogy. Using data from $n = 281$ participants ages 5 to 55, we show that "cooling off" does not only apply to the single dimension of randomness. Rather, development resembles an optimization process along multiple dimensions of learning (i.e., reward generalization, uncertainty-directed exploration, and decision temperature). What begins as large tweaks in the parameters that define learning during childhood plateaus and converges to efficient parameter constellations in adulthood. The developmental trajectory of human parameters is strikingly similar to several stochastic optimization algorithms, yet we observe intriguing differences in convergence. Notably, none of the optimization algorithms discovered reliably better regions of the strategy space than adult participants, suggesting a remarkable efficiency of human development.

Introduction

Human development has fascinated researchers of both biological and artificial intelligence alike. As the only known process that reliably produces human-level intelligence[1], there is broad interest in characterizing the developmental trajectory of human learning[2–4] and understanding why we observe specific patterns of change[5].

One influential hypothesis describes human development as a "cooling off" process[4,6,7], comparable to *simulated annealing*[8,9](SA). SA is a stochastic optimization algorithm named in analogy to a piece of metal that becomes harder to manipulate as it cools off. Initialized with high temperature, SA starts off highly flexible and likely to consider worse solutions as it explores the optimization landscape. But as the temperature cools down, the algorithm becomes increasingly greedy and more narrowly favoring only local improvements, eventually converging on an (approximately) optimal solution. Algorithms with similar cooling mechanisms, such as Stochastic Gradient Descent (SGD) and its discrete counterpart Stochastic Hill Climbing (SHC) are abundant in machine learning and have played a pivotal role in the rise of deep learning[10–13].

This analogy of stochastic optimization applied to human development is quite alluring: young children start off highly stochastic and flexible in generating hypotheses[4,14–16] and selecting actions[17], which gradually tapers off over the lifespan. This allows children to catch information that adults overlook[18], and learn unusual causal relationships adults might never consider[4,15]. Yet this high variability also results in large deviations from reward-maximizing behavior[3,19–22], with gradual improvements during development. Adults, in turn, are well-calibrated to their environment and quickly solve familiar problems, but at the cost of flexibility, since they experience difficulty adapting to novel circumstances[23–26].

While intuitively appealing, the implications and possible boundaries of the optimization analogy remain ambiguous without a clear definition of the process and a specification of what is being optimized. As a consequence, there is a need for a direct empirical test of the similarities and differences between human development and algorithmic optimization.

Perhaps the most direct interpretation is to apply "cooling off" to the single dimension of random decision temperature, controlling the amount of noise when selecting actions or sampling hypotheses[6,16,27], although alternative implementations are also possible[28,29]. Evidence from experimental

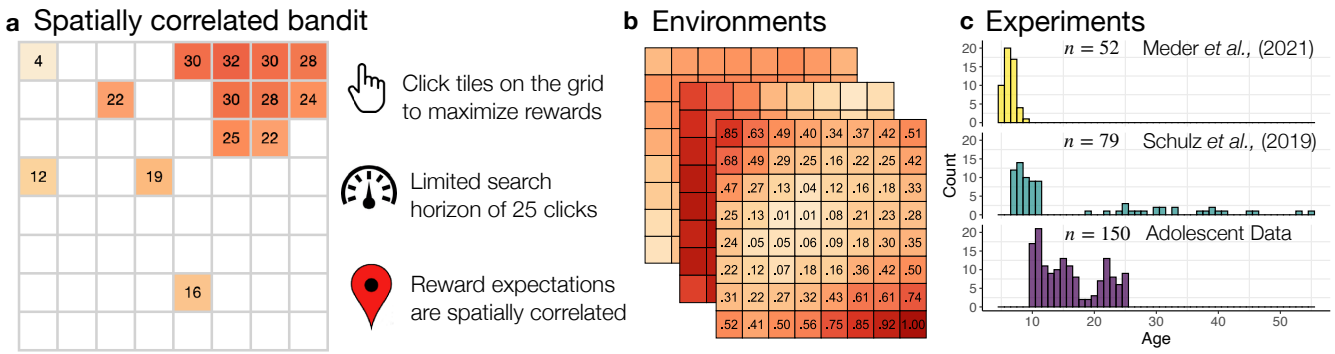

Figure 1. Experiments and model overview. **a**) Illustration of the task. **b**) Fully-revealed examples of the spatially correlated reward environments (showing expected reward), where nearby tiles tended to have similar rewards. **c**) Description of the three experiments, showing the number of participants and their age distribution (after filtering; see Methods).

studies suggest that young children are harder to predict than adults[17,30], implying greater stochasticity, which is amplified in neurodevelopmental disorders such as attention deficit hyperactivity disorder (ADHD)[28] and impulsivity[31]. However, this interpretation is only part of the story, since developmental differences in choice variability can be traced to changes affecting multiple aspects of learning and choice behavior. Aside from a decrease in randomness, development is also related to changes in more systematic, uncertainty-directed exploration[19,27,32], which is also reduced over the lifespan. Additionally, changes in how people generalize rewards to novel choices[27] and the integration of new experiences[33,34] affect how beliefs are formed and different actions are valued, also influencing choice variability. In sum, while decision noise certainly diminishes over the lifespan, this is only a single aspect of human development.

Alternatively, one could apply the "cooling off" metaphor to an optimization process in the space of learning strategies, which can be characterized across multiple dimensions of learning. Development might thus be framed as parameter optimization, which tunes the parameters of an individual's learning strategy, starting off by making large tweaks in childhood, followed by gradually lesser and more refined adjustments over the lifespan. In the stochastic optimization metaphor, training iterations of the algorithm become a proxy for age.

This interpretation connects the metaphor of stochastic optimization with Bayesian models of cognitive development, which share a common notion of gradual convergence[35,36]. In Bayesian models of development, individuals in early developmental stages possess broad priors and vague theories about the world, which become refined with experience[35]. Bayesian principles dictate that over time, novel experiences will have a lesser impact on future beliefs or behavior as one's priors become more narrow[36,37]. Observed over the lifespan, this process will result in large changes to beliefs and behavior early in childhood and smaller changes in later stages, implying a similar developmental pattern as the stochastic optimization metaphor. In sum, not only might the outcomes of behavior be more stochastic during childhood, but the changes to the parameters governing behavior might also be more stochastic in earlier developmental stages.

Goals and scope

In this work, we aim to resolve ambiguities around commonly used analogies to stochastic optimization in developmental psychology. While past work has compared differences in parameters between discrete age-groups in both structured[27,30] and unstructured reward domains[19,32,33], here we characterize the shape of developmental change across the lifespan, from ages 5 to 55. Instead of relying on verbal descriptions, we use formal computational models to clarify which cognitive processes are being tweaked during development through explicit commitments to free parameters. We then directly compare the trajectory of various optimization algorithms to age differences in those parameters, allowing us to finally put the metaphor to a direct empirical test.

Behavioral analyses show that rather than a uni-dimensional transition from exploration to exploitation, human development produces improvements in both faculties. Through computational models, we find simultaneous changes across multiple dimensions of learning, starting with large tweaks during childhood and plateauing in adulthood. We then provide direct empirical comparisons to multiple optimization algorithms as a meta-level analysis to describe changes in model parameters over the life span, where the best-performing algorithm is the most similar to human development. However, we also find notable differences in convergence between human development and algorithmic optimization. Yet, this disparity fails to translate into reliable differences in performance, suggesting a remarkable efficiency of human development.

Results

We analyze experimental data from $n = 281$ participants between the ages of 5 and 55, performing a spatially-correlated multi-armed bandit task that is both intuitive and richly complex (Fig. 1a)[38]. Participants were given a limited search horizon (25 choices) to maximize rewards by either selecting an unobserved or previously revealed tile on a 8×8 grid. Each

choice yielded normally distributed rewards, with reward expectations correlated based on spatial proximity (Fig. 1b), such that tiles close to one another tended to have similar rewards. Since the search horizon was significantly smaller than the number of unique options, generalization and efficient exploration was required to obtain high rewards.

Our dataset (Fig. 1c) combines openly available data from two previously published experiments[27,30] targeting children and adult participants ($n = 52$ and $n = 79$, respectively; after filtering), along with new unpublished data ($n = 150$) targeting the missing gap of adolescents. Although experimental designs differed in minor details (e.g., tablet vs. PC; see Methods), the majority of differences were removed by filtering out participants (e.g., assigned to a different class of reward environments). Reliability tests revealed no differences in performance, model accuracy, and parameter estimates for overlapping age groups across experiments (all $p > .128$ and $BF < .73$; see Fig. S1 and Table S1). Additionally, robust model and parameter recovery (Figs. S4-S6) provide high confidence in our ability to capture the key components of learning across the lifespan.

Behavioral Analyses

We first analyzed participant performance and behavioral patterns of choices (Fig. 2). We treat age as a continuous variable when possible, but also discretize participants into 7 similarly sized age groups ($n \in [30, 50]$). These behavioral results reveal clear age-related trends in learning and exploration captured by our task.

Performance

Participants monotonically achieved higher rewards as a function of age (Pearson correlation: $r = .51$, $p < .001$, $BF > 100$), with even the youngest age group (5-6 year olds) strongly outperforming chance (one-sample t-test: $t(29) = 5.1$, $p < .001$, $d = 0.9$, $BF > 100$; Fig. 2a). The learning curves in Figure 2b show average reward as a function of trial, revealing a similar trend, with older participants displaying steeper increases in average reward. Notably, the two youngest age groups (5-6 and 7-8 year olds) displayed decaying learning curves with decreasing average reward on later trials, suggesting a tendency to over-explore (supported by subsequent analyses below). We did not find any reliable effect of learning over rounds (Fig. S2).

We also analyzed maximum reward (up until a given trial) as a measure of exploration efficacy, where older participants reliably discovered greater maximum rewards (Kendall rank correlation: $r_\tau = .23$, $p < .001$, $BF > 100$) and showed steeper increases on a trial-by-trial basis (Fig. 2c). Thus, the reduction in the average reward acquired by the youngest age groups did not convert into improved exploration outcomes, measured in terms of maximum reward.

Behavioral patterns

Next, we looked at search patterns to better understand the behavioral signatures of age-related changes in exploration. The

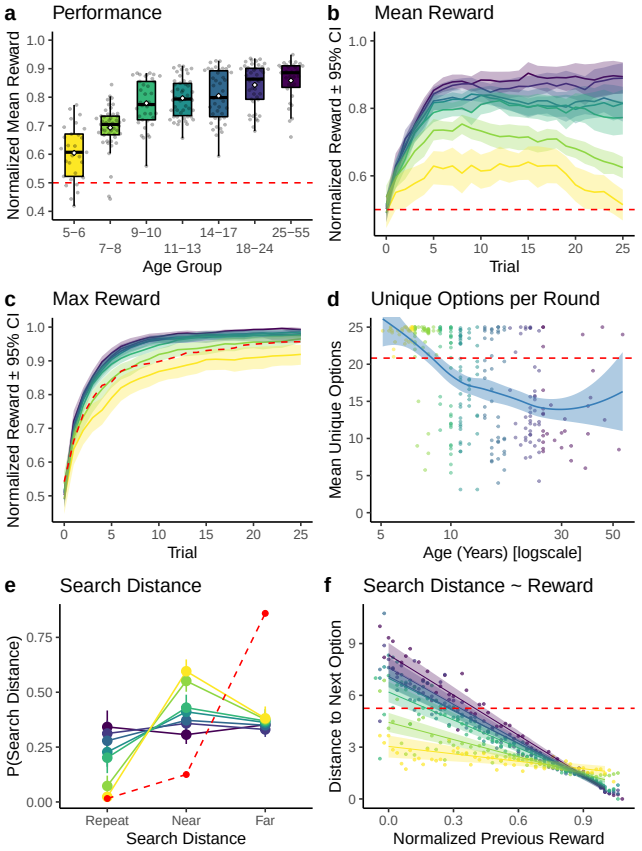

Figure 2. Behavioral results. **a**) Mean reward across age groups. Each dot is one participant, Tukey boxplots showing median and 1.5×IQR, with the white diamond indicating the group mean. The red dashed line indicates a random baseline (in all plots). The same colors are used to indicate age in all plots. **b**) Learning curves showing mean reward over trials, averaged across all rounds. Lines indicate group means, while the ribbons show the 95%CI. **c**) Learning curves showing maximum reward earned up until a given trial, averaged across all rounds. **d**) The number of unique options sampled per round as a function of age. Each dot is one participant, while the line and ribbon show a locally smoothed regression (±95% CI). **e**) The proportion of repeat, near (distance=1), and far (distance>1) choices as a function of age. Each dot indicates a group mean, while the error bars indicate the 95% CI. **f**) Search distance as a function of the previous reward value. Each line is the fixed effect of a hierarchical Bayesian regression (Table S3) with the ribbons indicating 95% CI. Each dot is the mean of the raw data.

youngest participants (5-6 year olds) sampled more unique options than chance (Wilcoxon signed-rank test: $Z = -4.7$, $p < .001$, $r = -.85$, $BF > 100$), but also less than the upper-bound on exploration (i.e., unique options on all 25 trials: $Z = -4.1$, $p < .001$, $r = -.76$, $BF > 100$). The number of unique options decreased strongly as a function of age ($r_\tau = -.33$, $p < .001$, $BF > 100$; Fig. 2d), consistent with the overall pattern of reduced exploration over the lifespan. Note that all participants were informed and tested about the fact they could repeat choices.

We then classified choices into repeat, near (distance=1) and far (distance>1), and compared this pattern of choices to a random baseline (red dashed line; Fig. 2e). 5-6 year olds started off with very few repeat choices (comparable to chance: $Z = 0.9$, $p = .820$, $r = .17$, $BF = .27$) and a strong

preference for near choices (more than chance: $Z = -4.6$, $p < .001$, $r = -.84$, $BF > 100$). Over the lifespan, the rate of repeat choices increased, while near decisions decreased, gradually reaching parity for 14-17 year olds (comparing repeat vs. near: $Z = -1.0$, $p = .167$, $r = -.15$, $BF = .46$) and remaining equivalent for all older age-groups (all $p > .484$, $BF < .23$). In contrast, the proportion of far choices remained unchanged over the lifespan ($r_\tau = -.08$, $p = .062$, $BF = .48$). These choice patterns indicate that even young children do not simply behave randomly, with the amount of randomness decreasing over time. Rather, younger participants exploit past options less than older participants (repeat choices), preferring instead to explore unknown tiles within a local radius (near choices). While the tendency to prefer exploring near rather than far options gradually diminished over the lifespan, this preference for local search distinguished participants of all age groups from the random model.

Lastly, we analyzed how reward outcomes influenced search distance using a Bayesian hierarchical regression (Fig. 2f; Table S3). This model predicted search distance as a function of the previous reward value and age group (including their interaction), with participants treated as random effects. This can be interpreted as a continuous analog to past work using a win-stay lose-shift strategy[17,38], and provides initial behavioral evidence for reward generalization. We found a negative linear relationship in all age groups, with participants searching locally following high rewards and searching further away after low rewards. This trend becomes stronger over the lifespan, with monotonically more negative slopes over the lifespan (see Table S3). While all age groups adapted their search patterns in response to reward, the degree of adaptation increased over the lifespan.

Behavioral summary

To summarize, younger children tended to explore unobserved tiles instead of exploiting options known to have good outcomes. This can be characterized as over-exploration since increased exploration did not translate into higher maximum rewards (Fig. 2c). Older participants explored less but more effectively, and were more responsive in adapting their search patterns to reward observations (Fig. 2f). We now turn to model-based analyses to complement these results with a more precise characterization of how the different mechanisms of learning and exploration change over the lifespan.

Model-Based Analyses

We conducted a series of reinforcement learning[39] analyses to characterize changes in learning over the lifespan. We first compared models in their ability to predict out-of-sample choices (Fig. 3b-c) and simulate human-like learning curves across age groups (Fig. 3d). We then analyzed the parameters of the winning model (Fig. 3e-f), which combined Gaussian process (GP) regression with Upper Confidence Bound (UCB) sampling (described below). These parameters allow us to describe how three different dimensions of learning change with age: *generalization* (λ; Eq. 2), uncertainty-directed *exploration* (β; Eq. 3), and decision *temperature* (τ; Eq. 4). We then compare the developmental trajectory of these parameters to different stochastic optimization algorithms (Fig. 4).

Modeling learning and exploration

We first describe the GP-UCB model (Fig. 3a) combining all three components of generalization, exploration, and decision temperature. We then lesion away each component to demonstrate all are necessary for describing behavior (Fig. 3b-c). We describe the key concepts below, while Figure 3a provides a visual illustration of the model (see Methods for details).

Gaussian process (GP) regression[40] provides a reinforcement learning model of value generalization[38], where past reward observations can be generalized to novel choices. Here, we describe generalization as a function of spatial location, where closer observations exhibit a larger influence. However, the same model can also be used to generalize based on the similarity of arbitrary features[41] or based on graph-structured relationships[42].

Given previously observed data $\mathcal{D}_t = \{\mathbf{X}_t, \mathbf{y}_t\}$ of choices $\mathbf{X}_t = [\mathbf{x}_1, \ldots, \mathbf{x}_t]$ and rewards $\mathbf{y}_t = [y_1, \ldots, y_t]$ at time t, the GP uses Bayesian principles to compute posterior predictions about the expected rewards r_t for any option $\mathbf{x}$:

$$p(r_t(\mathbf{x})|\mathcal{D}_t) \sim \mathcal{N}(m_t(\mathbf{x}), v_t(\mathbf{x})). \tag{1}$$

The posterior in Eq. 1 takes the form of a Gaussian distribution, allowing it to be fully characterized by posterior mean $m_t(\mathbf{x})$ and uncertainty $v_t(\mathbf{x})$ (i.e., variance; see Eqs. 6-7 for details and Figs. 3a for an illustration).

The posterior mean and uncertainty predictions critically depend on the choice of kernel function $k(\mathbf{x}, \mathbf{x}')$, for which we use a radial basis function (RBF) describing how observations from one option $\mathbf{x}$ generalize to another option $\mathbf{x}'$ as a function of their distance:

$$k(\mathbf{x}, \mathbf{x}') = \exp\left(-\frac{||\mathbf{x} - \mathbf{x}'||^2}{2\lambda^2}\right). \tag{2}$$

The model thus assumes nearby options generate similar rewards, with the level of similarity decaying exponentially over increased distances. The generalization parameter λ describes the rate at which generalization decays, with larger estimates corresponding to stronger generalization over greater distances.

We then use *Upper Confidence Bound* (UCB) sampling to describe the value of each option $q(\mathbf{x})$ as a weighted sum of expected reward $m(\mathbf{x})$ and uncertainty $v(\mathbf{x})$:

$$q(\mathbf{x}) = m(\mathbf{x}) + \beta\sqrt{v(\mathbf{x})}. \tag{3}$$

β captures uncertainty-directed exploration, determining the extent that uncertainty is valued positively, relative to exploiting options with high expectations of reward.

Lastly, we use a softmax policy to translate value $q(\mathbf{x})$ into choice probabilities:

$$p(\mathbf{x}) \propto \exp(q(\mathbf{x})/\tau) \tag{4}$$

The decision temperature τ controls the amount of random exploration. Larger values for τ introduce more choice stochasticity, where $\tau \to \infty$ converges on a random policy.

Lesioned models

To ensure all components of the GP-UCB model play a necessary role in capturing behavior, we created model variants lesioning away each component. The λ lesion model removed the capacity for generalization, by replacing the GP component with a Bayesian reinforcement learning model that assumes independent reward distributions for each option (Eqs. 8-11). The β lesion model removed the capacity for uncertainty-directed exploration by fixing $\beta = 0$, thus valuing options solely based on expectations of reward $m(\mathbf{x})$. Lastly, the τ lesion model swapped the softmax policy for an epsilon-greedy policy, as an alternative form of choice stochasticity: with probability $p(\varepsilon)$ a random option is sampled, and with probability $p(1-\varepsilon)$ the option with the highest UCB value is sampled (Eq. 12).

Model comparison

We fit all models using leave-one-round-out cross validation (see Methods). We then conducted hierarchical Bayesian model selection[43] to compute the protected exceedence probability (pxp) for describing which model is most likely in the population. We found that GP-UCB was the best model for each individual age group and also aggregated across all data (Fig 3a). There is still some ambiguity between models in the 5-6 year old group, but this quickly disappears in all subsequent age groups ($pxp_{\text{GP-UCB}} > .99$). Figure 3b describes the out-of-sample predictive accuracy of each model as a continuous function of age, where a pseudo-R^2 provides an intuitive comparison to random chance (Eq. 13). Intuitively, $R^2 = 0$ indicates chance-level predictions and $R^2 = 1$ indicates theoretically perfect predictions. While there is again some ambiguity among 5-6 year olds, GP-UCB quickly dominates and remains the best model across all later ages.

Aside from only predicting choices, we also simulated learning curves for each model (using median participant parameter estimates) and compared them against human performance for each age group (Fig. 3c). The full GP-UCB model provides the best description across all age groups, although the β lesion model also produces similar patterns. However, only GP-UCB by virtue of the exploration bonus β is able to recreate the decaying learning curves for 5-6 and 7-8 year olds.

Altogether, these results reveal that all three components of generalization (λ), uncertainty-directed exploration (β), and decision temperature (τ) play a vital role in describing behavior. Next, we analyze how each of these parameters change over the lifespan.

Parameters

We use both regression and similarity analyses to interpret age-related changes in GP-UCB parameters. The regression (Fig. 3e) modeled age-related changes in the log-transformed parameters using a multivariate Bayesian changepoint regression[44] (see Methods). This approach models the relationship between age and each parameter as separate linear functions separated by an estimated changepoint ω, at which point the regression slope changes from b_1 to b_2 (Eq. 15). Using leave-one-out cross-validation, we established that this simple changepoint model predicted all GP-UCB parameters better than linear or complex regression models up to fourth-degree polynomials (both with and without log-transformed variables and compared against lesioned intercept-only variants; see Tables S5-S6).

The regression analysis (Fig. 3e) revealed how all parameters changed rapidly during childhood (all b_1 CIs different from 0), but then plateaued such that there were no credible changes in parameters after the estimated change point (all b_2 CIs overlapped with 0; see Table S7). More specifically, generalization increased ($b_1(\lambda)$ = 0.08 [0.02,0.26]) until around 13 years of age ($\omega(\lambda)$ = 12.7 [7.70,19.80]), whereas there were sharp decreases in directed exploration ($b_1(\beta)$ = -0.39 [-0.79, -0.13]) and decision temperature ($b_1(\tau)$ = -0.59 [-1.05,-0.25]), until around 9 ($\omega(\beta)$ = 9.10 [7.44,11.40]) and 8 ($\omega(\tau)$ = 7.74 [6.88,8.77]) years of age, respectively.

In a multivariate similarity analysis, we computed the pairwise similarity of all parameter estimates between participants (Kendall's τ), which we then averaged over age groups (Fig. 3f). This shows that older participants were more similar to each other than younger participants (Fig. 3f inset), suggesting development produces a convergence towards a more similar set of parameters. Whereas older participants achieved high rewards using similar learning strategies, younger participants tended to over-explore and acquired lower rewards, but each in their own fashion, with more diverse strategies.

These results highlight how development produces changes to all parameters governing learning, not only a unidimensional reduction in random sampling. An initially steep but plateauing rate of change across model parameters is broadly consistent with the metaphor of stochastic optimization in the space of learning strategies (Fig. 3e). The increasing similarity in participants' parameters again speaks for a developmental process that gradually converges on a configuration of learning parameters (Fig. 3f), which can also be used to generate better performance (Fig. 3d).

Comparison of human and algorithmic trajectories

Beyond qualitative analogies, we now present a direct empirical comparison between human development and stochastic optimization. We first computed a fitness landscape (Fig. S7) across 1 million combinations of plausible parameter values of the GP-UCB model (see Methods), with each parameter combination yielding a mean reward based on 100 simulated rounds. We then simulated different optimization algorithms on the fitness landscape, using each of the cross-validated parameter estimates of the 5-6 year old age group as initialization points. Specifically, we tested simulated annealing (SA) and stochastic hill climbing (SHC) in combination with three

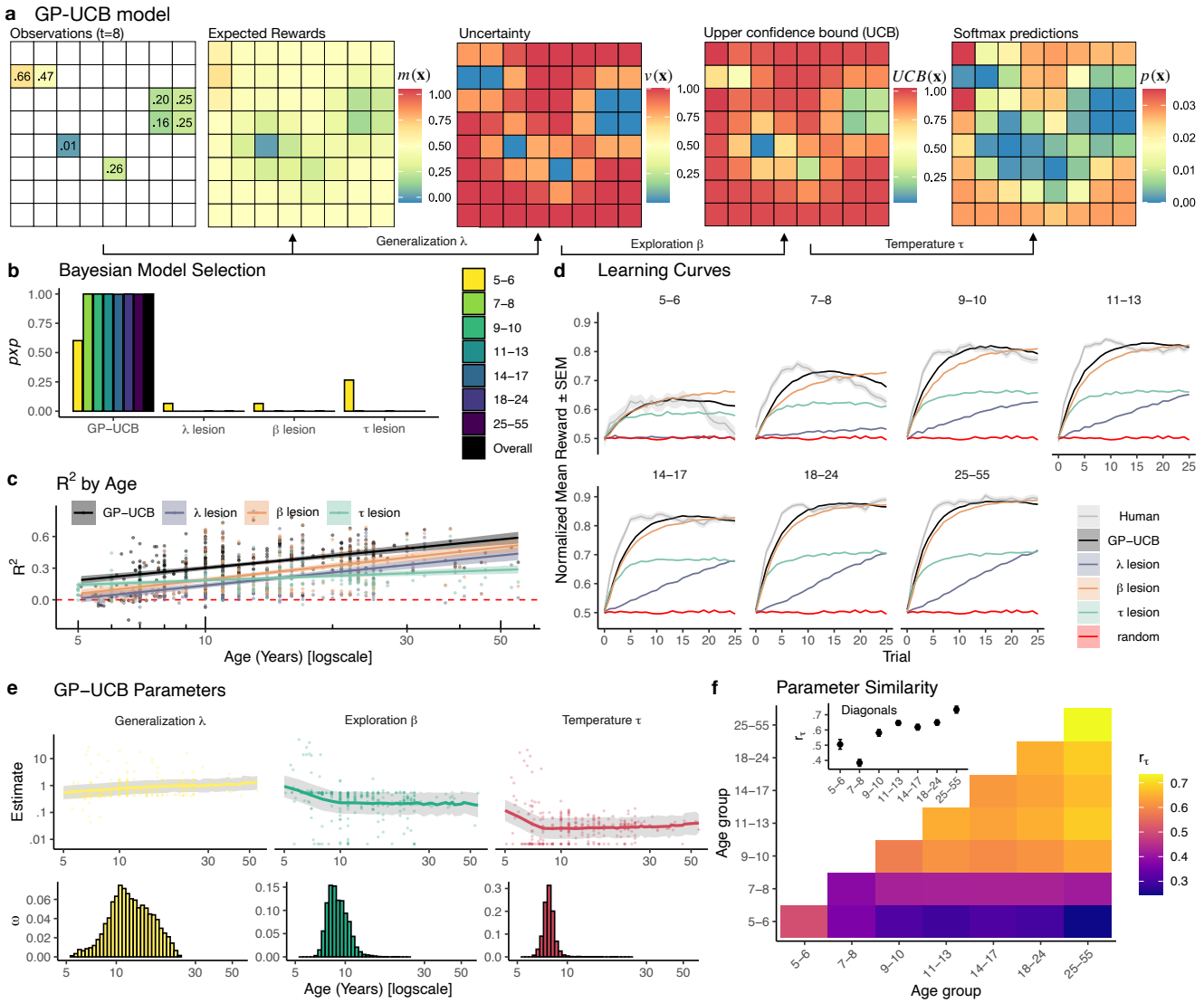

Figure 3. Model results. **a**) Illustration of the GP-UCB model based on observations at the 8th trial (showing normalized reward). We use Gaussian process (GP) regression as a psychological model of reward generalization[38], making Bayesian estimates about the expected rewards and uncertainty for each option. The free parameter λ (Eq. 2) controls the extent that past observations *generalize* to new options. The expected rewards $m(\mathbf{x})$ and uncertainty estimates $v(\mathbf{x})$ are combined using Upper Confidence Bound (UCB) sampling (Eq. 3) to produce a valuation for each option. The *exploration* bonus β governs the value of exploring uncertain options relative to exploiting high reward expectations. Lastly, UCB values are entered into a softmax function (Eq. 4) to make probabilistic predictions about where the participant will search next. The decision *temperature* parameter τ governs the amount of random (undirected) exploration. **b**) Hierarchical Bayesian model selection, where *pxp* defines the probability of each model being predominant in the population (see Fig. S2 and Table S3 for more details). **c**) Predictive accuracy (R^2) as a function of age. Each dot is a participant and the lines and ribbons show the slope (± 95% CI) of a linear regression. **d**) Simulated learning curves, using participant parameter estimates. Human data illustrates the mean (± 95% CI), while model simulations report the mean. **e**) Top: Participant parameter estimates as a function of age. Each dot is a single participant, with the line and ribbon showing the posterior predictions from a Bayesian changepoint regression model. Bottom: Posterior distribution of which age the changepoint (ω) is estimated to occur. **f**) Similarity-matrix of parameter estimates. Using Kendall's rank correlation (r_τ), we report the similarity of parameter estimates both within and between age-groups. The within age-group similarities (diagonals) are also visualized in the inset plot, where error bars indicate the 95% CI.

common cooling schedules (fast cooling, exponential cooling, and linear cooling; see Methods). Intuitively, SA uses rejection sampling to preferentially select better solutions in the fitness landscape (Eq. 16), with higher optimization temperatures relaxing this preference. SHC is a discrete analogue of stochastic gradient descent, selecting new solutions proportional to their relative fitness (Eq. 17), with higher optimization temperatures making it more likely to select lower fitness solutions.

While we do not attempt to curve-fit the exact cooling schedule that best describes human development, we observe that fast and exponential cooling generally performed better than linear cooling (Fig. 4a). The metaphor therefore holds: we do not observe linear changes in development, but rather rapid initial changes during childhood, followed by a gradual plateau and convergence. Yet remarkably, neither SA nor SHC converged on reliably better solutions than adult 25-55 year old participants (SA-fast cooling: $t(149) = -0.4$, $p =$

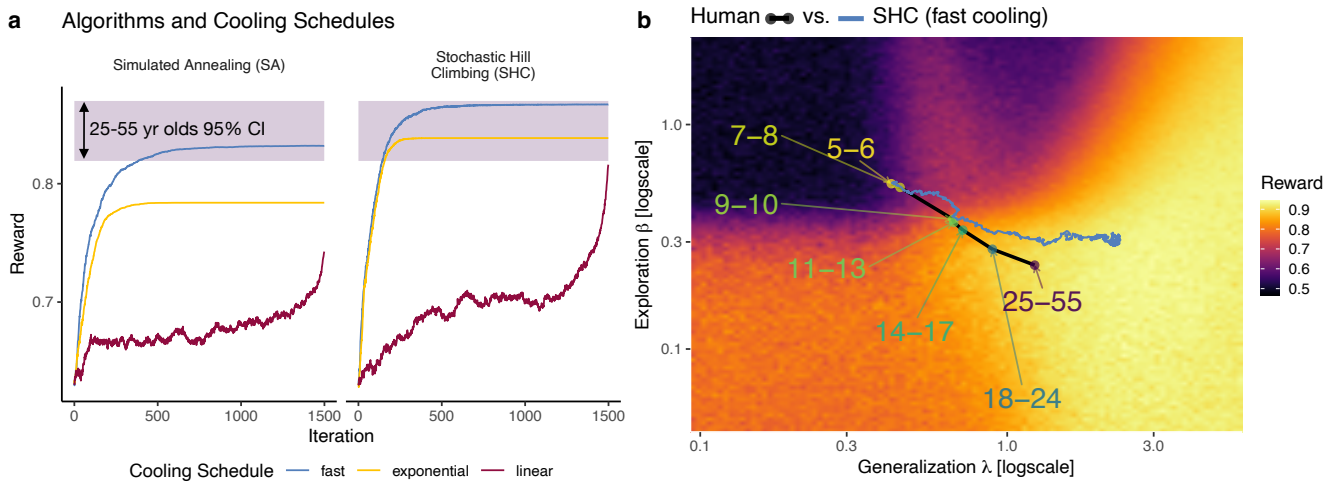

Figure 4. Developmental Trajectory. **a**) Mean reward in each iteration for simulated annealing (SA) and stochastic hill climbing (SHC) algorithms, combined with fast, exponential, and linear cooling schedules. The shaded purple band indicates the 95% CI of human performance in the 25-55 age group. **b**) Comparison of human and algorithm trajectories, focusing on the best performing SHC-fast cooling algorithm. The annotated dots show the median parameter estimates of each age group, while the blue line shows the trajectory of the optimization algorithm (median overall all simulations). This 2D illustration focuses on changes in generalization λ and directed-exploration β (see Fig. S6 for all algorithms and all parameter comparisons), with the underlying fitness landscape depicted using the median τ estimate across all human data ($\bar{\tau} = .03$).

.675, $d = 0.08$, $BF = .23$; SHC-fast cooling: $t(149) = 0.8$, $p = .447$, $d = 0.2$, $BF = .27$).

Figure 4b compares the developmental trajectory of human participants (labeled dots) to the trajectory of the best performing SHC (fast cooling) algorithm (blue line; see Fig. S8 for all algorithms and all parameter comparisons and Fig. S9 for variability of trajectories). We focus on changes in generalization and exploration parameters since rewards decrease monotonically with increased decision temperature. Particularly for younger age groups, age-related changes in parameters follow a similar trajectory as the optimization algorithms. However, a notable divergence emerges around adolescence (ages 14-17).

To concretely relate human and algorithmic trajectories, we estimated the same changepoint regression model (Fig. 3e) on the sequence of algorithmic parameters from the SHC (fast cooling) algorithm (see Fig. S10 for details). This revealed a similar pattern of rapid change before the changepoint with all b_1 slopes having the same direction as humans, followed by a plateau of b_2 slopes around 0 (Fig. S10a; see Table S8).

This analysis also allows us to quantify convergence differences between human development and stochastic optimization. For a given dataset (human vs. algorithm) and a given parameter (λ, β, τ), we use the respective upper 95% CI of ω estimates as a threshold for convergence (Fig. S10b). Comparing a matched sample of parameter estimates after the convergence threshold, we find that human generalization λ and directed-exploration β parameters converged at lower values than the algorithm (λ: $U = 2740$, $p < .001$, $r_\tau = -.38$, $BF > 100$; β: $U = 10114$, $p < .001$, $r_\tau = -.19$, $BF > 100$), while decision temperature τ was not credibly higher or lower ($U = 22377$, $p = .188$, $r_\tau = .05$, $BF = .12$; Fig. S10c).

Since these deviations nevertheless fail to translate into reliable differences in performance, this may point towards resource rational constraints on human development[45,46]: aside from only optimizing for the best performance, the cognitive costs of different strategies may also be considered (see Discussion).

Discussion

From a rich data set of $n = 281$ participants ages 5 to 55, our results reveal human development does not only "cool off" in the search for rewards or hypotheses, but also in the search for the best learning strategy. Thus, the stochastic optimization metaphor best applies to a multivariate optimization of all parameters of a learning model, rather than only a decrease in randomness when selecting actions or hypotheses. What begins as large tweaks to the cognitive mechanisms of learning and exploration during childhood, gradually plateaus and converges in adulthood (Fig. 3e-f). This process is remarkably effective, resembling the trajectory of the best-performing stochastic optimization algorithm (SHC-fast cooling; Fig. 4) as it optimizes the psychologically interpretable parameters of a Bayesian reinforcement learning model (GP-UCB). While there are notable differences in the solutions human development and stochastic optimization converged upon, none of the algorithms achieved reliably better performance than adult human participants (25-55 year olds; Fig. 4a). This work provides important insights into the nature of developmental changes in learning and offers normative explanations for why we observe these specific developmental patterns.

Rather than a uni-dimensional transition from exploration to exploitation over the lifespan[25], we observe refinements in both the ability to explore (Fig. 2c) and exploit (Fig. 2f), with monotonic improvements in both measures as a function of age. While even 5-6 year olds perform better than chance (Fig. 2a), exploration becomes more effective over the lifespan, as larger reward values are discovered despite sampling

fewer unique options (Fig. 2c-d). Meanwhile, exploitation becomes more responsive, with older participants adapting their search distance more strongly based on reward outcomes (Fig. 2e). This resembles a developmental refinement of a continuous win-stay lose-shift heuristic[17,38], and is consistent with the hypothesis that people use heuristics more efficiently as they age[47]. These results also reaffirm past work showing a reduction of stochasticity over the lifespan[4,14,16], but expand the scope of developmental changes across multiple dimensions of learning.

With a reinforcement learning model (GP-UCB), we characterize age-related changes in learning through the dimensions of *generalization* (λ), uncertainty-directed *exploration* (β), and decision *temperature* (τ). All three dimensions play an essential role in predicting choices (Fig. 3b-c) and simulating realistic learning curves across all ages (Fig. 3d), with recoverable models and parameter estimates (Figs S4-S6).

Changes in all parameters occur rapidly during childhood (increase in generalization and decrease in both exploration and decision temperature), but then plateaus around adolescence (Fig. 3e). Younger participants tend to be more diverse, whereas adults are more similar to one another, with continued convergence of parameter estimates until adulthood (25-55 year olds; Fig. 3f). Both the reduction of age-related differences and the increasing similarity of parameters support the analogy of development as a stochastic optimization process, which gradually converges upon an (approximately optimal) configuration of learning parameters.

Our direct comparison between the developmental trajectory of human parameters to various stochastic optimization algorithms (Fig. 4) revealed both striking similarities and intriguing differences. The best-performing algorithm (SHC with fast cooling) also most resembles the parameter trajectory of human development (Fig. S8), suggesting that optimization provides a useful characterization of developmental changes in learning strategy.

However, there are also limitations to the metaphor, and it should be noted that different parameters are optimal in different contexts[48,49]. Other developmental studies using reinforcement learning models suggest older participants may display more optimal parameters in general[3], by being better able to adapt their strategies to task demands. This raises the question of whether children indeed have less optimal parameters *per se* or are simply slower when adapting to the task. We partially address this possibility by analyzing performance over rounds, where we found no reliable age-related differences in learning over rounds (Fig. S2). Thus, it seems unlikely that given more time to adapt to the task (e.g., adding more rounds), children would register more optimal parameters.

Nevertheless, suboptimality of task-specific parameters does not suggest that younger individuals are maladaptive from a developmental context. Rather, development prepares children to learn about the world more generally, beyond the scope of any specific experimental paradigm or computational model. In line with the stochastic optimization analogy, younger children could try diverse strategies that our model does not account for, which then registers as sub-optimal parameter estimates. This is consistent with the result that the predictive accuracy of the model generally increases over the lifespan (i.e., R^2: Fig. 3c).

We also observed intriguing differences in the parameters that humans converged on compared to the algorithm trajectories, with adult participants displaying lower generalization and less uncertainty-directed exploration (Fig. S10). Yet remarkably, none of the optimization algorithms achieved significantly better performance than adult participants (Fig. 4). Thus, these differences might point towards cognitive costs, which are not justified by any increased performance benefits. Generalization over a greater extent may require remembering and performing computations over a larger set of past observations[42,50], which is why some GP approximations reduce the number of inputs to save computational costs[51]. Similarly, deploying uncertainty-directed exploration is also associated with increased cognitive costs[52], and can be systematically diminished through working memory load[53] or time pressure[54] manipulations.

Limitations and future directions

One limitation of our analyses is that we rely on cross-sectional rather than longitudinal data, observing changes in learning not only across the lifespan but also across individuals. Yet despite the advantages of longitudinal studies, it might not be appropriate in this setting because we would be unable to distinguish between performance improvement due to cognitive development and practice. Having participants repeatedly interact with the same task at different stages of development could conflate task-specific changes in reward learning with domain-general changes in their learning strategy. Yet future longitudinal analyses may be possible using a richer paradigm. For instance, modeling how we learn intuitive theories about the world[55] or compositional programs[56] as a search process in some latent hypothesis space. The richness of these domains may allow similar dimensions of learning to be measured from sufficiently distinct tasks administered at different developmental stages.

While we have characterized behavioral changes in learning using the distinct and recoverable parameters of a reinforcement learning model, future work is needed to relate these parameters to the development of specific neural mechanisms. Existing research provides some promising candidates. Blocking dopamine D2-receptors has been shown to impact stimulus generalization[57], selectively modulating similarity-based responses in the hippocampus. Similar multi-armed bandit tasks have linked the frontopolar cortex and the intraparietal sulcus to exploratory decisions[58], where more specifically, the right frontopolar cortex has been causally linked to uncertainty-directed exploration[59], which can be selectively inhibited via transcranial magnetic stimulation.

Stochastic optimization also allows for "re-heating"[8] by

adding more flexibility in later optimization stages. Reheating is often used in dynamic environments or when insensitivities of the fitness landscape can cause the algorithm to get stuck. Since deviations from the algorithm trajectories start in adolescence, this may coincide with a second window of developmental plasticity during adolescence[60,61]. While we observed relatively minor changes in the parameters governing individual learning, plasticity in adolescents is thought to specifically target social learning mechanisms[7,62]. Thus, different aspects of development may fall under different cooling schedules and similar analyses should also be applied to other learning contexts.

Additionally, our participant sample is potentially limited by a WEIRD bias[63], where the relative safety of developmental environments may promote more exploration. While we would expect to find a similar qualitative pattern in more diverse cultural settings, different expectations about the richness or predictability of environments may promote quantitatively different levels of each parameter. Indeed, previous work using a similar task but with risky outcomes found evidence for a similar generalization mechanism, but a different exploration strategy that prioritized safety[64].

Finally, our research also has implications for the role of the environment in maldaptive development. Our comparison to stochastic optimization suggests, in line with life history theory[65] and empirical work in rodents and humans[4,61,66], that childhood and adolescence are sensitive periods for configuring learning and exploration parameters. Indeed, adverse childhood experiences have been shown to reduce exploration and impair reward learning?. Organisms utilize early life experience to configure strategies for interacting with their environment, which for most species remain stable throughout the life span[67]. Once the configuration of learning strategies has cooled off, there is less flexibility for adapting to novel circumstances in later developmental stages. In the machine learning analogy we have used, some childhood experiences can produce a mismatch between training and test environments, where deviations from the expected environment has been linked to a number of psychopathologies[68]. Such a mismatch would set the developmental trajectory towards regions of the parameter space that are poorly suited for some features of the adult environment, but may provide hidden benefits for other types problems more similar to the ones encountered during development[69]. Rather than only focusing on adult phenotypes at a single point in time, accounting for adaptation and optimization over the lifespan provide a more complete understanding of developmental processes.

Conclusions

Scientists often look to statistical and computational tools for explanations and analogies[70]. With recent advances in machine learning and artificial intelligence, these tools are increasingly vivid mirrors into the nature of human cognition and its development. We can understand idiosyncrasies of hypothesis generation through Monte Carlo sampling[71], individual learning through optimization[72–74], and development as programming or "hacking"[56]. An important advantage of computational explanations is that they offer direct empirical demonstrations, instead of remaining as vague, verbal comparisons. Here, we provided such a demonstration, and added much-needed clarity to commonly used analogies of stochastic optimization in developmental psychology.

Methods

Experiments

We combined open data from two previously published experiments (Meder et al[30] and Schulz et al[27]) targeting children and adult participants, together with new unpublished data targeting adolescent participants (see below). The experimental designs differed in a few details, the majority of which were removed by filtering participants. The combined and filtered data consisted of 281 participants between the ages of 5 and 55 (M_{age}=14.46, SD=8.61, 126 female). Informed consent was obtained from all participants or their legal guardians prior to participation.

Generic materials and procedure

All participants performed a spatially-correlated bandit task[38] on a 8×8 grid of 64 options (i.e., tiles). A random tile was revealed at the beginning of each round, with participants given a limited search horizon of 25 trials to acquire as many cumulative rewards as possible by either choosing new or previously revealed tiles. After each round, participants were rewarded a maximum of five stars reflecting their performance relative to always selecting the optimal tile. The number of stars earned in each round stayed visible until the end of the experiment.

When choosing a tile, participants earned rewards corrupted by normally distributed noise $\varepsilon \sim \mathcal{N}(0,1)$. Reward expectations were spatially-correlated across the grid, such that nearby tiles had similar reward expectations (described below). Earned rewards were depicted numerically along with a corresponding color (only colors in Meder et al.,[30]; see below), with darker colors depicting higher rewards. Figure 1a provides a screenshot of the task and Figure 1b depicts the distribution of rewards on a fully revealed environment.

All experiments (after filtering, see below) used the same set of underlying 40 reward environments, which define a bivariate function on the grid, mapping each tile's location on the grid to an expected reward value. The environments were generated by sampling from a multivariate Gaussian distribution $\sim \mathcal{N}(0,\Sigma)$, with covariance matrix Σ defined by a RBF kernel (Eq. 2) with $\lambda = 4$. In each round, a new environment was chosen without replacement from the list of environments. To prevent participants from knowing when they found the highest reward, a different maximum range was sampled from a uniform distribution $\sim \mathcal{U}(30,40)$ for each round and all reward values were rescaled accordingly. The rescaled rewards were then shifted by $+5$ to avoid reward observations below 0. Hence, the effective rewards ranged from 5 to 45, with a different maximum in each round. All experiments included an initial training round designed to interactively explain the nature of the task, and ended with a bonus round in which they were asked to predict the rewards of unseen tiles. All analyses exclude the training and bonus rounds.

Differences across experiments

Participants from the Meder et al[30] and Schulz et al[64] studies were recruited from museums in Berlin and paid with stickers (Meder

et al[30]) or with money (Schulz et al[64]) proportional to their performance in the task. The new adolescent data includes 150 participants (M_{age}=16.1, SD=4.97, 69 female) who completed the task at the Max Planck Institute for Human Development in Berlin along with a battery of 10 other decision-making tasks on a desktop computer. These participants were given a fixed payment of €10 per hour. This study was approved by the Ethics Committee of the Max Planck Institute for Human Development (A 2018/23).

Both Meder et al[30] and Schulz et al[64] studies used a between-subject manipulation of the strength of rewards correlations (smooth vs. rough environments: $\lambda_{smooth} = 4$, $\lambda_{rough} = 1$). Because only minimal differences in model parameters were found in previous studies[27,30,38], the rough condition was omitted in the adolescent sample. Thus, we filtered out all participants assigned to the rough condition such that only participants assigned to the smooth environments were included in the final sample. Lastly, both Schulz et al[64] and the adolescent experiment used ten rounds, while Meder et al[30] included only six rounds to avoid lapses in attention in the younger age group. In addition, numerical depictions of rewards were removed in the Meder et al[30] experiment, and participants were instructed to focus on the colors (deeper red indicating more rewards) to avoid difficulties with reading large numbers.

After filtering, the remaining differences in modality (tablet vs. computer), incentives (stickers vs. variable money vs. fixed money), number of rounds (six vs. ten), and visualization of rewards (numbers+colors vs. only colors) did not result any differences in performance (Fig. S1a), model fits (Fig. S1b), or parameter estimates (Fig. S1c).

Computational models

Gaussian process generalization

Gaussian process (GP) regression[40] provides a non-parametric Bayesian framework for function learning, which we use as a method of value generalization[38]. We use the GP to infer a value functions $f : \mathcal{X} \rightarrow \mathbb{R}^n$ mapping input space $\mathcal{X}$ (all possible options on the grid) to a real-valued scalar outputs r (reward expectations). The GP performs this inference in a Bayesian manner, by first defining a prior distribution over functions $p(r_0)$, which is assumed to be multivariate Gaussian:

$$p\big(r_0(\mathbf{x})\big) \sim \mathcal{GP}\left(m(\mathbf{x}), k(\mathbf{x},\mathbf{x}')\right), \tag{5}$$

with the prior mean $m(\mathbf{x})$ defining the expected output of input $\mathbf{x}$, and with covariance defined by the kernel function $k(\mathbf{x},\mathbf{x}')$, for which we use an RBF kernel (Eq. 2). Per convention, we set the prior mean to zero, without loss of generality[40].

Conditioned on a set of observations $\mathcal{D}_t = \{\mathbf{X}_t, \mathbf{y}_t\}$, the GP computes a posterior distribution $p(r_t(\mathbf{x}_*)|\mathcal{D}_t)$ (Eq 1) for some new input $\mathbf{x}_*$, which is also Gaussian, with posterior mean and variance defined as:

$$m(\mathbf{x}_*|\mathcal{D}_t) = \mathbf{k}_{*,t}^\top(\mathbf{K} + \sigma_\varepsilon^2\mathbf{I})^{-1}\mathbf{y}_t \tag{6}$$

$$v(\mathbf{x}_*|\mathcal{D}_t) = k(\mathbf{x}_*,\mathbf{x}_*) - \mathbf{k}_{*,t}^\top(\mathbf{K} + \sigma_\varepsilon^2\mathbf{I})^{-1}\mathbf{k}_{*,t} \tag{7}$$

$\mathbf{k}_{*,t} = k(\mathbf{X}_t,\mathbf{x}_*)$ is the covariance matrix between each observed input and the new input $\mathbf{x}_*$ and $\mathbf{K} = k(\mathbf{X}_t,\mathbf{X}_t)$ is the covariance matrix between each pair of observed inputs. $\mathbf{I}$ is the identity matrix and σ_ε^2 is the observation variance, corresponding to assumed i.i.d. Gaussian noise on each reward observation.

Lesioned models

The λ lesion model removes the capacity for generalization, by replacing the GP with a *Bayesian Mean Tracker* (BMT) as a reinforcement learning model that learns reward estimates for each option independently using the dynamics of a Kalman filter with time-invariant rewards. Reward estimates are updated as a function of prediction error, thus the BMT can be interpreted as Bayesian variant of the classic Rescorla-Wagner model[75,76] and has been used to describe human behavior in a variety of learning and decision-making tasks[54,77,78].

The BMT also defines a Gaussian prior distribution of the reward expectations, but does so independently for each option $\mathbf{x}$:

$$p\big(r_0(\mathbf{x})\big) \sim \mathcal{N}\big(m_0(\mathbf{x}), v_0(\mathbf{x})\big). \tag{8}$$

The BMT computes an equivalent posterior distribution for the expected reward for each option (Eq. 1), also in the form of a Gaussian, but where the posterior mean $m_t(\mathbf{x})$ and posterior variance $v_t(\mathbf{x})$ are defined independently for each option and computed by the following updates:

$$m_{t+1}(\mathbf{x}) = m_t(\mathbf{x}) + \delta_t(\mathbf{x})G_t(\mathbf{x})\big(y_t(\mathbf{x}) - m_t(\mathbf{x})\big) \tag{9}$$

$$v_{t+1}(\mathbf{x}) = v_t(\mathbf{x})\big(1 - \delta_t(\mathbf{x})G_t(\mathbf{x})\big) \tag{10}$$

Both updates use $\delta_t(\mathbf{x}) = 1$ if option $\mathbf{x}$ was chosen on trial t, and $\delta_t(\mathbf{x}) = 0$ otherwise. Thus, the posterior mean and variance are only updated for the chosen option. The update of the mean is based on the prediction error $y_t(\mathbf{x}) - m_t(\mathbf{x})$ between observed and anticipated reward, while the magnitude of the update is based on the Kalman gain $G_t(\mathbf{x})$:

$$G_t(\mathbf{x}) = \frac{v_t(\mathbf{x})}{v_t(\mathbf{x}) + \theta_\varepsilon^2}, \tag{11}$$

analogous to the learning rate of the Rescorla-Wagner model. Here, the Kalman gain is dynamically defined as a ratio of variance terms, where $v_t(\mathbf{x})$ is the posterior variance estimate and θ_ε^2 is the error variance, which (analogous to the GP) models the level of noise associated with reward observations. Smaller values of θ_ε^2 thus result in larger updates of the mean.

The β lesion simply fixes $\beta = 0$, making the valuation of options solely defined by the expected rewards $q(\mathbf{x}) = m(\mathbf{x})$.

The τ lesion model swaps the softmax policy (characterized by decision temperature τ) for an epsilon-greedy policy[39], since it is not feasible to simply remove the softmax component or fix $\tau = 0$ making it an argmax policy (due to infinite log loss from zero probability predictions). Instead, we use take the opportunity to compare the softmax policy against epsilon-greedy as an alternative mechanism of random exploration[28]. We still combine epsilon-greedy with GP and UCB components, but rather than choosing options proportional to their UCB value, the τ lesion estimates ε as a parameter controlling the probability of choosing an option at random vs. the highest UCB option:

$$p(\mathbf{x}) = \begin{cases} \arg\max q(\mathbf{x}), & \text{with probability } 1-\varepsilon \\ 1/64, & \text{with probability } \varepsilon \end{cases} \tag{12}$$

Model cross-validation

Each model was fit using leave-one-round-out cross validation for each individual participant using maximum likelihood estimation (MLE). Model fits are described using negative log likelihoods (nLLs) summed over all out-of-sample predictions, while individual participant parameter estimates are based on averaging over the

cross-validated MLEs. Figure 3c reports model fits in terms of a pseudo-R^2, which compares the out-of-sample nLLS for each model k against a random model:

$$R^2 = 1 - \frac{\log \mathcal{L}(M_k)}{\log \mathcal{L}(M_{random})} \tag{13}$$

Changepoint regression

We use a hierarchical Bayesian changepoint model to quantify univariate changes in model parameters as a function of age:

$$\text{estimate} \sim \mathcal{N}(\mu_{age}, \sigma^2), \tag{14}$$

$$\begin{aligned}\mu_{age} = b_0 + b_1 * (age - \omega) * I(age < \omega) \\ + b_2 * (age - \omega) * I(age > \omega).\end{aligned} \tag{15}$$

$I(\cdot)$ is an indicator function, b_0 is the intercept, and ω is the age at which the slope b_1 changes to b_2. We included random intercepts for different experiments. To account for potential outliers in the parameter estimates, we used a student-t likelihood function as a form of robust regression. Table S5 depicts a model comparison between this robust regression reported in the main text, a regression with a Gaussian likelihood that attenuates skew by log transforming the dependent variable and regressions with a Gaussian likelihood that does not account for skew in the dependent variable. Using approximate leave one out cross validation we found that the robust regression consistently fit the parameter distributions best.

Fitness landscape

We used Tukey's fence to define credible interval for each GP-UCB parameter [λ, β, τ] based on participant estimates and created a grid of 100 equally-sized log-space intervals for each parameter. This defines a space of plausible learning strategies corresponding to 1 million parameter combinations. We then ran 100 simulations of the GP-UCB model for each parameter combination (sampling one of the 40 reward environments with replacement each time) and computed the mean reward across iterations (Fig. S7).

Optimization algorithms

Using this fitness landscape defined across learning strategies, we simulated the trajectories of various optimization algorithms. Specifically, we tested simulated annealing[4,9] (SA) and stochastic hill climbing[12,13] (SHC), the latter of which provides a discrete analogue to the better known stochastic gradient descent method commonly used to optimize neural networks[10,11]. Each optimization algorithm (SA vs. SHC) was combined with one of three common cooling schedules[79] defining how the optimization temperature (temp) changes as a function of the iteration number i. Fast cooling uses $\text{temp}_i = 1/(1+i)$, exponential cooling use $\text{temp}_i = \exp(-i^{1/3})$, and linear cooling uses $\text{temp}_i = 1 - (i+1)/\max(i)$. As the optimization temperature decreases over iterations, there is a general decrease in the amount of randomness or stochasticity.

SA is a stochastic sampling algorithm, which is more likely to select solutions with lower fitness when the optimization temperature is high. After initialization, SA iteratively selects a random neighboring solution s_{new} in the fitness landscape (i.e., one step in the grid of 1 million parameter combinations), and either deterministically accepts it if it corresponds to higher fitness than the current solution s_{old}, otherwise, it accepts worse solutions with probability:

$$p(\text{accept}) \propto \exp(\frac{s_{\text{new}} - s_{\text{old}}}{\text{temp}_i}), \tag{16}$$

where temp_i is the current optimization temperature.

SHC is similar, but considers all neighboring solutions $s' \in \mathcal{S}_{\text{neighbors}}$ and selects a new solution proportional its fitness:

$$p(s') \propto \exp(s'/\text{temp}_i) \tag{17}$$

For each combination of optimization algorithm and cooling function, we simulated optimization trajectories over 1500 iterations. Each simulated was initialized on each of the cross-validated parameter estimates of all participants of the youngest age group as starting points. This resulted in 120 (30 participants $\times$ 4 rounds of cross validation) trajectories for each combination of algorithm and cooling schedule.

Data and Code Availability

Code and data are publicly available at https://github.com/AnnaGiron/developmental_trajectory.

References

1. Tenenbaum, J. B., Kemp, C., Griffiths, T. L. & Goodman, N. D. How to grow a mind: Statistics, structure, and abstraction. *science* **331**, 1279–1285 (2011).
2. Moran, R. J., Symmonds, M., Dolan, R. J. & Friston, K. J. The brain ages optimally to model its environment: evidence from sensory learning over the adult lifespan. *PLoS computational biology* **10**, e1003422 (2014). DOI 10.1371/journal.pcbi.1003422.
3. Nussenbaum, K. & Hartley, C. A. Reinforcement learning across development: What insights can we draw from a decade of research? *Dev. cognitive neuroscience* **40**, 100733 (2019).
4. Gopnik, A. *et al.* Changes in cognitive flexibility and hypothesis search across human life history from childhood to adolescence to adulthood. *Proc. Natl. Acad. Sci.* **114**, 7892–7899 (2017).
5. Walasek, N., Frankenhuis, W. E. & Panchanathan, K. Sensitive periods, but not critical periods, evolve in a fluctuating environment: a model of incremental development. *Proc. Royal Soc. B* **289**, 20212623 (2022).
6. Gopnik, A., Griffiths, T. L. & Lucas, C. G. When younger learners can be better (or at least more open-minded) than older ones. *Curr. Dir. Psychol. Sci.* **24**, 87–92 (2015).
7. Ciranka, S. & van den Bos, W. Adolescent risk-taking in the context of exploration and social influence. *Dev. Rev.* **61**, 100979 (2021).
8. Du, K.-L. & Swamy, M. N. S. Simulated annealing. In Du, K.-L. & Swamy, M. N. S. (eds.) *Search and Optimization by Metaheuristics: Techniques and Algorithms Inspired by Nature*, 29–36 (Springer International Publishing, Cham, 2016).
9. Kirkpatrick, S., Gelatt, C. D. & Vecchi, M. P. Optimization by simulated annealing. *science* **220**, 671–680 (1983).
10. Robbins, H. & Monro, S. A stochastic approximation method. *The annals mathematical statistics* 400–407 (1951).
11. Bottou, L., Curtis, F. E. & Nocedal, J. Optimization methods for large-scale machine learning. *Siam Rev.* **60**, 223–311 (2018).
12. Rieskamp, J., Busemeyer, J. R. & Laine, T. How do people learn to allocate resources? comparing two learning theories. *J. Exp. Psychol. Learn. Mem. Cogn.* **29**, 1066 (2003).
13. Moreno-Bote, R., Ramírez-Ruiz, J., Drugowitsch, J. & Hayden, B. Y. Heuristics and optimal solutions to the breadth–depth dilemma. *Proc. Natl. Acad. Sci.* **117**, 19799–19808 (2020).

14. Buchsbaum, D., Bridgers, S., Skolnick Weisberg, D. & Gopnik, A. The power of possibility: Causal learning, counterfactual reasoning, and pretend play. *Philos. Transactions Royal Soc. B: Biol. Sci.* **367**, 2202–2212 (2012).

15. Lucas, C. G., Bridgers, S., Griffiths, T. L. & Gopnik, A. When children are better (or at least more open-minded) learners than adults: Developmental differences in learning the forms of causal relationships. *Cognition* **131**, 284–299 (2014).

16. Denison, S., Bonawitz, E., Gopnik, A. & Griffiths, T. L. Rational variability in children's causal inferences: The sampling hypothesis. *Cognition* **126**, 285–300 (2013).

17. Bonawitz, E., Denison, S., Gopnik, A. & Griffiths, T. L. Win-stay, lose-sample: A simple sequential algorithm for approximating bayesian inference. *Cogn. psychology* **74**, 35–65 (2014).

18. Sumner, E. *et al.* The exploration advantage: Children's instinct to explore allows them to find information that adults miss. *PsyArXiv* (2019). DOI 10.31234/osf.io/h437v.

19. Somerville, L. H. *et al.* Charting the expansion of strategic exploratory behavior during adolescence. *J. experimental psychology: general* **146**, 155 (2017).

20. Jepma, M., Schaaf, J. V., Visser, I. & Huizenga, H. M. Uncertainty-driven regulation of learning and exploration in adolescents: A computational account. *PLoS computational biology* **16**, e1008276 (2020).

21. Palminteri, S., Kilford, E. J., Coricelli, G. & Blakemore, S.-J. The computational development of reinforcement learning during adolescence. *PLoS computational biology* **12**, e1004953 (2016).

22. Rosenbaum, G. M., Venkatraman, V., Steinberg, L. & Chein, J. M. The influences of described and experienced information on adolescent risky decision making. *Dev. Rev.* **47**, 23–43 (2018).

23. Baltes, P. B. Theoretical propositions of life-span developmental psychology: On the dynamics between growth and decline. *Dev. Psychol.* (1987).

24. Baltes, P. B., Staudinger, U. M. & others. Lifespan psychology: Theory and application to intellectual functioning. *Annu. review* (1999).

25. Gopnik, A. Childhood as a solution to explore–exploit tensions. *Philos. Transactions Royal Soc. B* **375**, 20190502 (2020).

26. Gopnik, A. Scientific thinking in young children: theoretical advances, empirical research, and policy implications. *Science* **337**, 1623–1627 (2012).

27. Schulz, E., Wu, C. M., Ruggeri, A. & Meder, B. Searching for rewards like a child means less generalization and more directed exploration. *Psychol. Sci.* **30**, 1561–1572 (2019). DOI 10.1177/0956797619863663.

28. Dubois, M. *et al.* Tabula-rasa exploration decreases during youth and is linked to adhd symptoms. *BioRxiv* (2020).

29. Feng, S. F., Wang, S., Zarnescu, S. & Wilson, R. C. The dynamics of explore–exploit decisions reveal a signal-to-noise mechanism for random exploration. *Sci. reports* **11**, 1–15 (2021).

30. Meder, B., Wu, C. M., Schulz, E. & Ruggeri, A. Development of directed and random exploration in children. *Dev. Sci.* e13095 (2021). DOI 10.1111/desc.13095.

31. Dubois, M. & Hauser, T. U. Value-free random exploration is linked to impulsivity. *Nat. communications* **13**, 1–17 (2022).

32. Blanco, N. J. & Sloutsky, V. M. Systematic exploration and uncertainty dominate young children's choices. *Dev. Sci.* **24**, e13026 (2021).

33. Van den Bos, W., Cohen, M. X., Kahnt, T. & Crone, E. A. Striatum–medial prefrontal cortex connectivity predicts developmental changes in reinforcement learning. *Cereb. cortex* **22**, 1247–1255 (2012).

34. Blanco, N. J. *et al.* Exploratory decision-making as a function of lifelong experience, not cognitive decline. *J. Exp. Psychol. Gen.* **145**, 284 (2016).

35. Tenenbaum, J. B., Kemp, C., Griffiths, T. L. & Goodman, N. D. How to grow a mind: statistics, structure, and abstraction. *Science* **331**, 1279–1285 (2011).

36. Stamps, J. A. & Frankenhuis, W. E. Bayesian models of development. *Trends Ecol. Evol.* **31**, 260–268 (2016).

37. Frankenhuis, W. E. & Panchanathan, K. Balancing sampling and specialization: an adaptationist model of incremental development. *Proc. Biol. Sci.* **278**, 3558–3565 (2011).

38. Wu, C. M., Schulz, E., Speekenbrink, M., Nelson, J. D. & Meder, B. Generalization guides human exploration in vast decision spaces. *Nat. Hum. Behav.* **2**, 915—-924 (2018). DOI 10.1038/s41562-018-0467-4.

39. Sutton, R. S. & Barto, A. G. *Reinforcement learning: An introduction* (MIT press, 2018).

40. Rasmussen, C. E. & Williams, C. Gaussian processes for machine learning the mit press. *Cambridge, MA* (2006).

41. Wu, C. M., Schulz, E., Garvert, M. M., Meder, B. & Schuck, N. W. Similarities and differences in spatial and non-spatial cognitive maps. *PLOS Comput. Biol.* **16**, 1–28 (2020). DOI 10.1371/journal.pcbi.1008149.

42. Wu, C. M., Schulz, E. & Gershman, S. J. Inference and search on graph-structured spaces. *Comput. Brain & Behav.* **4**, 125–147 (2021). DOI 10.1007/s42113-020-00091-x.

43. Rigoux, L., Stephan, K. E., Friston, K. J. & Daunizeau, J. Bayesian model selection for group studies—revisited. *Neuroimage* **84**, 971–985 (2014).

44. Simonsohn, U. Two lines: A valid alternative to the invalid testing of U-Shaped relationships with quadratic regressions. *Adv. Methods Pract. Psychol. Sci.* **1**, 538–555 (2018).

45. Bhui, R., Lai, L. & Gershman, S. J. Resource-rational decision making. *Curr. Opin. Behav. Sci.* **41**, 15–21 (2021).

46. Lieder, F. & Griffiths, T. L. Resource-rational analysis: Understanding human cognition as the optimal use of limited computational resources. *Behav. Brain Sci.* **43** (2020).

47. Reyna, V. F. & Brainerd, C. J. Fuzzy-trace theory: An interim synthesis. *Learn. Individ. Differ.* **7**, 1–75 (1995).

48. Eckstein, M. K., Wilbrecht, L. & Collins, A. G. E. What do reinforcement learning models measure? interpreting model parameters in cognition and neuroscience. *Curr Opin Behav Sci* **41**, 128–137 (2021).

49. Ciranka, S. *et al.* Asymmetric reinforcement learning facilitates human inference of transitive relations. *Nat Hum Behav* **6**, 555–564 (2022).

50. Gershman, S. J. & Daw, N. D. Reinforcement learning and episodic memory in humans and animals: an integrative framework. *Annu. review psychology* **68**, 101–128 (2017).

51. Liu, H., Ong, Y.-S., Shen, X. & Cai, J. When Gaussian process meets big data: A review of scalable GPs. *IEEE Transactions on Neural Networks Learn. Syst.* (2020).

52. Otto, A. R., Knox, W. B., Markman, A. B. & Love, B. C. Physiological and behavioral signatures of reflective exploratory choice. *Cogn. Affect. & Behav. Neurosci.* **14**, 1167–1183 (2014).

53. Cogliati Dezza, I., Cleeremans, A. & Alexander, W. Should we control? the interplay between cognitive control and information integration in the resolution of the exploration-exploitation dilemma. *J. Exp. Psychol. Gen.* **148**, 977 (2019).

54. Wu, C. M., Schulz, E., Pleskac, T. J. & Speekenbrink, M. Time pressure changes how people explore and respond to uncertainty. *Scientific Reports* **12**, 1–14 (2022). DOI https://doi.org/10.1038/s41598-022-07901-1.

55. Gerstenberg, T. & Tenenbaum, J. B. Intuitive Theories. In *The Oxford Handbook of Causal Reasoning* (Oxford University Press, 2017). DOI 10.1093/oxfordhb/9780199399550.013.28.

56. Rule, J. S., Tenenbaum, J. B. & Piantadosi, S. T. The child as hacker. *Trends cognitive sciences* **24**, 900–915 (2020).

57. Kahnt, T. & Tobler, P. N. Dopamine regulates stimulus generalization in the human hippocampus. *Elife* **5**, e12678 (2016).

58. Daw, N. D., O'doherty, J. P., Dayan, P., Seymour, B. & Dolan, R. J. Cortical substrates for exploratory decisions in humans. *Nature* **441**, 876–879 (2006).

59. Zajkowski, W. K., Kossut, M. & Wilson, R. C. A causal role for right frontopolar cortex in directed, but not random, exploration. *Elife* **6**, e27430 (2017).

60. Laube, C., van den Bos, W. & Fandakova, Y. The relationship between pubertal hormones and brain plasticity: Implications for cognitive training in adolescence. *Dev. Cogn. Neurosci.* **42**, 100753 (2020).

61. Dahl, R. E., Allen, N. B., Wilbrecht, L. & Suleiman, A. B. Importance of investing in adolescence from a developmental science perspective. *Nature* **554**, 441–450 (2018).

62. Blakemore, S.-J. & Mills, K. L. Is adolescence a sensitive period for sociocultural processing? *Annu. Rev. Psychol.* **65**, 187–207 (2014).

63. Henrich, J., Heine, S. J. & Norenzayan, A. Most people are not weird. *Nature* **466**, 29–29 (2010).

64. Schulz, E., Wu, C. M., Huys, Q. J., Krause, A. & Speekenbrink, M. Generalization and search in risky environments. *Cogn. Sci.* **42**, 2592–2620 (2018). DOI 10.1111/cogs.12695.

65. Del Giudice, M., Gangestad, S. W. & Kaplan, H. S. Life history theory and evolutionary psychology. (2016).

66. Lin, W. C. *et al.* Transient food insecurity during the juvenile-adolescent period affects adult weight, cognitive flexibility, and dopamine neurobiology. *Curr. Biol.* (2022).

67. Frankenhuis, W. E., Panchanathan, K. & Nettle, D. Cognition in harsh and unpredictable environments. *Curr. Opin.* (2016).

68. Humphreys, K. L. & Zeanah, C. H. Deviations from the expectable environment in early childhood and emerging psychopathology. *Neuropsychopharmacology* **40**, 154–170 (2015).

69. Young, E. S., Frankenhuis, W. E., DelPriore, D. J. & Ellis, B. J. Hidden talents in context: Cognitive performance with abstract versus ecological stimuli among adversity-exposed youth. *Child Dev.* (2022).

70. Gigerenzer, G. From tools to theories: A heuristic of discovery in cognitive psychology. *Psychol. Rev.* **98**, 254–267 (1991).

71. Dasgupta, I., Schulz, E. & Gershman, S. J. Where do hypotheses come from? *Cognitive Psychology* **96**, 1–25 (2017).

72. Barry, D. N. & Love, B. C. Human learning follows the dynamics of gradient descent (2021).

73. Ritz, H., Leng, X. & Shenhav, A. Cognitive control as a multivariate optimization problem. *J. Cogn. Neurosci.* 1–23 (2022).

74. Hennig, J. A. *et al.* How learning unfolds in the brain: toward an optimization view. *Neuron* **109**, 3720–3735 (2021).

75. Rescorla, R. A. & Wagner, A. R. A theory of pavlovian conditioning: Variations in the effectiveness of reinforcement and nonreinforcement. *Class. conditioning II: Curr. research theory* **2**, 64–99 (1972).

76. Gershman, S. J. A unifying probabilistic view of associative learning. *PLoS Comput. Biol* **11**, e1004567 (2015).

77. Gershman, S. J. Deconstructing the human algorithms for exploration. *Cognition* **173**, 34–42 (2018).

78. Dayan, P., Kakade, S. & Montague, P. R. Learning and selective attention. *Nat. neuroscience* **3**, 1218–1223 (2000).

79. Nourani, Y. & Andresen, B. A comparison of simulated annealing cooling strategies. *J. Phys. A: Math. Gen.* **31**, 8373 (1998).

80. Rouder, J. N., Speckman, P. L., Sun, D., Morey, R. D. & Iverson, G. Bayesian t tests for accepting and rejecting the null hypothesis. *Psychon. Bull. & Rev.* **16**, 225–237 (2009).

81. van Doorn, J., Ly, A., Marsman, M. & Wagenmakers, E.-J. Bayesian latent-normal inference for the rank sum test, the signed rank test, and Spearman's ρ. *arXiv preprint arXiv:1712.06941* (2017).

82. Jeffreys, H. *The Theory of Probability* (Oxford, UK: Oxford University Press, 1961).

83. Ly, A., Verhagen, J. & Wagenmakers, E.-J. Harold jeffreys's default bayes factor hypothesis tests: Explanation, extension, and application in psychology. *J. Math. Psychol.* **72**, 19–32 (2016).

84. van Doorn, J., Ly, A., Marsman, M. & Wagenmakers, E.-J. Bayesian inference for kendall's rank correlation coefficient. *The Am. Stat.* **72**, 303–308 (2018).

85. Wilson, R. C. & Collins, A. G. Ten simple rules for the computational modeling of behavioral data. *Elife* **8**, e49547 (2019).

86. Vehtari, A., Gelman, A. & Gabry, J. Practical bayesian model evaluation using leave-one-out cross-validation and WAIC. *arXiv [stat.CO]* (2015).

87. Bürkner, P.-C. Advanced Bayesian multilevel modeling with the R package brms. *The R J.* **10**, 395–411 (2018). DOI 10.32614/RJ-2018-017.

Acknowledgments

We thank Kou Murayama, Michiko Sakaki, Philipp Schwartenbeck, Mani Hamidi, and Ryu Uchiyama for helpful feedback and Chantal Wysocki for data collection. CMW is supported by the German Federal Ministry of Education and Research (BMBF): Tübingen AI Center, FKZ: 01IS18039A and funded by the Deutsche Forschungsgemeinschaft (DFG, German Research Foundation) under Germany's Excellence Strategy–EXC2064/1–390727645.

Author Contributions

CMW, SC, and APG conceived the study with feedback from all authors. SC collected the data using materials provided by CMW. CMW, APG, and SC performed the analyses. CMW, SC, and APG wrote the paper, with feedback from all authors.

Competing financial interests

The authors declare no competing financial interests.

Supplementary Information for

Developmental changes resemble stochastic optimization

Anna Giron, Simon Ciranka, Eric Schulz, Wouter van den Bos, Azzurra Ruggeri, Björn Meder, & Charley M. Wu

Comparability Across Experiments

To assess whether the data from the different experiments are equivalent, we compared participants' performance (Fig. S1a), the mean predictive accuracy of the GP-UCB model (Fig. S1b), and parameter estimates for all parameters of the GP-UCB model (Fig. S1c). Both, frequentist statistics and Bayes factors (BF) are reported (see Statistics). We compared data from the different experiments for overlapping age ranges: participants between 7-9 from Experiment 1 ($n = 36$) and Experiment 2 ($n = 22$) and participants older than 20 years from Experiment 1 ($n = 24$) and Experiment 3 ($n = 43$). Participants younger than or equal to 20 years were excluded from the comparisons, because of expected developmental changes over the course of adolescence.

Plot S1a shows participants' performance separated by experiments. We found no difference in performance for both age groups (children between 7-9: $t(56) = 1.5$, $p = .128$, $d = 0.4$, $BF = .73$; adults older than 20: $t(65) = -0.7$, $p = .460$, $d = 0.2$, $BF = .33$). Additionally, a comparison of the predictive accuracy showed no differences in model performance between different experiments (children between 7-9: $t(56) = 0.7$, $p = .467$, $d = 0.2$, $BF = .34$; adults older than 20: $t(65) = -0.9$, $p = .394$, $d = 0.2$, $BF = .35$; see Figure S1b). Furthermore, we compared parameter estimates for overlapping age ranges. Since parameter estimates are bounded above 0, we performed rank-based tests (Mann–Whitney U) to look for differences in parameter estimates across different experiments. The results are reported in Table S1 and Figure S1c), where we did not find any significant differences.

From these results, we concluded that data from the different experiments can be integrated and used for joint analyses of behavioral changes over the lifespan.

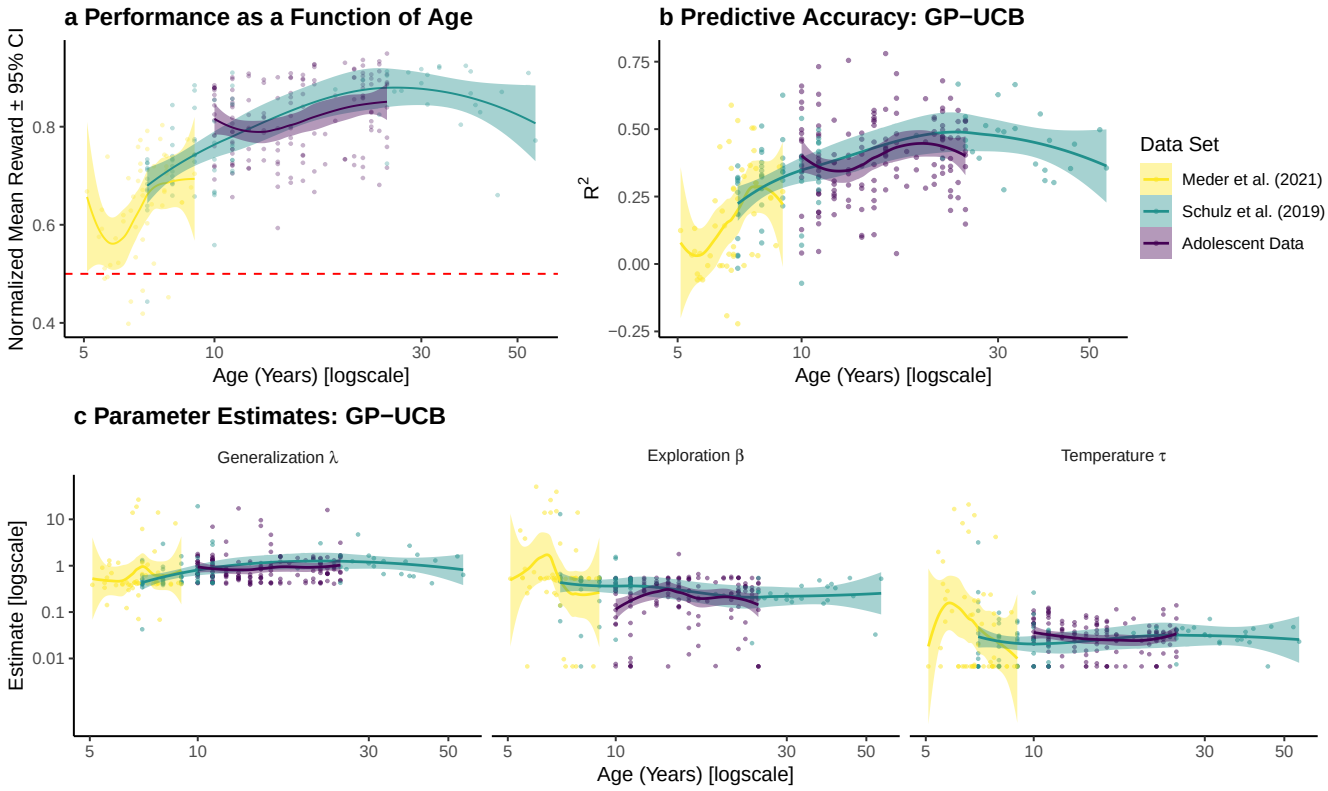

Figure S1. Reliability checks. **a** Average reward as a function of age, lines show the smoothed conditional means and 95% confidence interval for data from each experiment. Dots represent the mean reward for each participant and the red dashed line shows the performance of a random choice model. **b**) Predictive accuracy of the GP-UCB model as a function of age and **c**) Parameter estimates of the GP-UCB model as a function of age, separated by experiment. Lines show the smoothed conditional means and 95% confidence interval and dots represent the predictive accuracy per participant.)

Statistics

Comparisons

Both frequentist and Bayesian statistics are reported throughout this paper. Frequentist tests are reported as Student's t-tests (specified as either paired or independent) for parametric comparisons, while the Mann-Whitney U test or Wilcoxon signed-rank test are used for non-parametric comparisons (for independent samples or paired samples, respectively). Each of these tests are

Table S1. Comparison of GP-UCB parameter estimates across different experiments

Parameter	**(Age)**	U	p	r_τ	BF
Generalization λ	(7-9)	390	.930	−.01	.29
Generalization λ	(>20)	438	.313	−.10	.38
Exploration β	(7-9)	373	.721	−.04	.29
Exploration β	(>20)	554	.626	.05	.28
Temperature τ	(7-9)	422	.685	.05	.31
Temperature τ	(>20)	496	.800	−.03	.27

Note: We conducted non-parametric two-sample tests to compare the estimates for children between 7-9 from Experiment 1 ($n = 36$) and Experiment 2 ($n = 22$) and the estimates for adult participants older than 20 from Experiment 1 ($n = 24$) and Experiment 3 ($n = 43$).

accompanied by a Bayes factors (BF) to quantify the relative evidence the data provides in favor of the alternative hypothesis (H_A) over the null (H_0). For parametric comparisons, this is done using the default two-sided Bayesian t-test for either independent or dependent samples, using a Jeffreys-Zellner-Siow prior with its scale set to $\sqrt{2}/2$, as suggested by Ref[80]. For non-parametric comparisons, the Bayesian test is based on performing posterior inference over the test statistics (Kendall's r_τ for the Mann-Whitney-U test and standarized effect size $r = \frac{Z}{\sqrt{N}}$ for the Wilcoxon signed-rank test) and assigning a prior using parametric yoking[81]. This leads to a posterior distribution for for Kendall's r_τ or the standarized effect size r, which yields an interpretable Bayes factor via the Savage-Dickey density ratio test. The null hypothesis posits that the parameters do not differ between the two groups or from the baseline, while the alternative hypothesis posits an effect and assigns an effect size using a Cauchy distribution with the scale parameter set to $1/\sqrt{2}$. All statistical tests are non-directional as defined by a symmetric prior.

Correlations

For testing linear correlations with Pearson's r, the Bayesian test is based on Jeffreys[82] test for linear correlation and assumes a shifted, scaled beta prior distribution $B(\frac{1}{k}, \frac{1}{k})$ for r, where the scale parameter is set to $k = \frac{1}{3}$, following Ref[83]. For testing rank correlations with Kendall's tau, the Bayesian test is based on parametric yoking to define a prior over the test statistic[84], and performing Bayesian inference to arrive at a posterior distribution for r_τ. The Savage-Dickey density ratio test is used to produce an interpretable Bayes Factor. Note that when performing group comparisons of correlations computed at the individual level, we report the mean correlation and the statistics of a single-sample t-test comparing the distribution of z-transformed correlation coefficients to $\mu = 0$.

Supplementary Behavioral results

Learning over rounds regression

We used a Bayesian hierarchical regression model to analyze if performance changed over multiple rounds of the task. We model participants as random intercepts, with rounds, age groups, and their interaction as fixed effects with random slopes. Figure S2 and Table S2 provide the model results. They show no effect of round and no reliable interactions between round and age group.

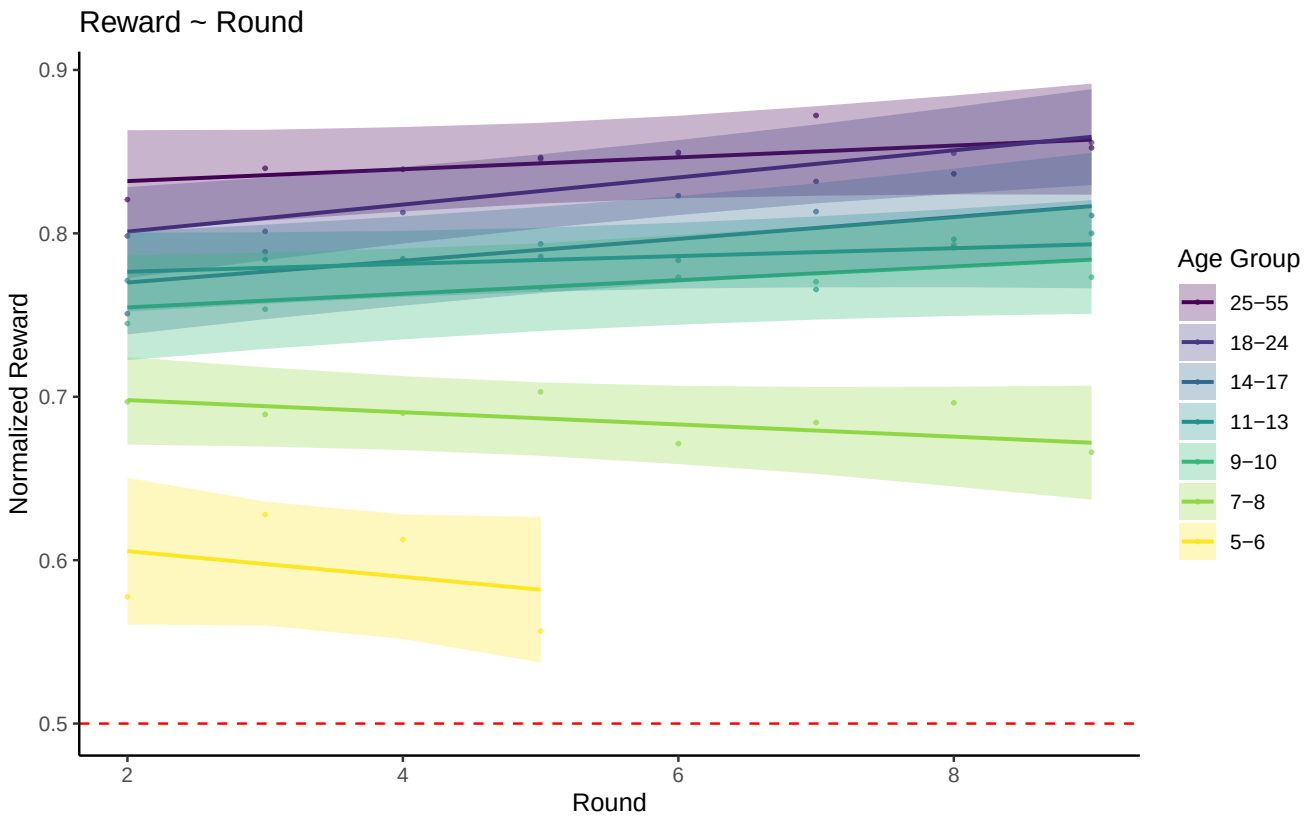

Figure S2. Learning over rounds. Reward as a function of rounds. Each line is the fixed effect of a hierarchical Bayesian regression (Table S2) with the ribbons indicating 95% CI. Dots show the group mean in each round and the red dashed line indicates a random baseline. We found no effect of round and no reliable interactions between round and age group.

Table S2. Bayesian linear multilevel regression: learning over rounds as a function of age group.

	Estimate	**95% HDI**
Intercept	0.82	[0.79, 0.86]
Round	0.00	[-0.00, 0.01]
Age group 18-24	-0.04	[-0.09, -0.01]
Age group 14-17	-0.07	[-0.12, -0.01]
Age group 11-13	-0.05	[-0.10, -0.00]
Age group 9-10	-0.08	[-0.13, -0.02]
Age group 7-8	-0.12	[-0.17, -0.07]
Age group 5-6	-0.20	[-0.28, -0.12]
Round× Age group 18-24	0.00	[-0.00, 0.01]
Round × Age group 14-17	0.00	[-0.00, 0.01]
Round × Age group 11-13	-0.00	[-0.01, 0.01]
Round × Age group 9-10	0.00	[-0.01, 0.01]
Round × Age group 7-8	-0.01	[-0.02, 0.00]
Round × Age group 5-6	-0.01	[-0.03, 0.01]
Random Effects		
σ^2	0.01	
τ_{00}	0.00	
$\tau_{11\ \text{round}}$	0.00	
$\tau_{11\ \text{age group 18-24}}$	0.00	
$\tau_{11\ \text{age group 14-17}}$	0.00	
$\tau_{11\ \text{age group 11-13}}$	0.00	
$\tau_{11\ \text{age group 9-10}}$	0.00	
$\tau_{11\ \text{age group 7-8}}$	0.00	
$\tau_{11\ \text{age group 5-6}}$	0.01	
ICC	0.28	
N	281	
Observations	2040	
Bayesian R^2	0.48	

Note: Posterior mean and 95% highest density interval (HDI) are reported for all coefficients. Age group 25-55 is the reference level for the categorical variable age group. σ^2 indicates the individual-level variance and τ the variation between individual intercepts and average intercept. ICC is the intraclass correlation coefficient.

Search distance regression

We used a Bayesian hierarchical linear regression model to analyze the relation between the obtained reward and search distance in the next trial. In this model, participants were treated as random effects. Age group, reward obtained in the previous round, and their interaction were treated as fixed effects with random slopes. Table S3 provides the model results. They indicate an effect of age group, older participants showed higher search distances. Additionally, we found an effect of previous reward on search distance, higher rewards lead to sampling of closer tiles. Furthermore, results suggest an interaction between age group and previously obtained reward: older participants adjust their search distance more in line with the previously obtained reward than younger participants do.

Table S3. Bayesian linear multilevel regression: search distance as a function of previous reward.

	Estimate	**95% HDI**
Intercept	8.35	[7.64, 9.04]
Previous reward	-7.76	[-8.51, -6.99]
Age group 18-24	-0.75	[-1.65, 0.17]
Age group 14-17	-1.25	[-2.18, -0.33]
Age group 11-13	-1.35	[-2.22, -0.44]
Age group 9-10	-2.15	[-3.05, -1.23]
Age group 7-8	-3.91	[-4.82, -3.01]
Age group 5-6	-5.30	[-6.25, -4.36]
Previous reward × Age group 18-24	0.70	[-0.31, 1.67]
Previous reward × Age group 14-17	1.28	[0.27, 2.29]
Previous reward × Age group 11-13	1.47	[0.48, 2.42]
Previous reward × Age group 9-10	2.37	[1.33, 3.39]
Previous reward × Age group 7-8	4.43	[3.45, 5.44]
Previous reward × Age group 5-6	6.32	[5.21, 7.42]
Random Effects		
σ^2	3.17	
τ_{00}	3.52	
$\tau_{11\ \text{previous reward}}$	4.24	
$\tau_{11\ \text{age group 18-24}}$	0.04	
$\tau_{11\ \text{age group 14-17}}$	0.16	
$\tau_{11\ \text{age group 11-13}}$	0.10	
$\tau_{11\ \text{age group 9-10}}$	0.33	
$\tau_{11\ \text{age group 7-8}}$	0.05	
$\tau_{11\ \text{age group 5-6}}$	0.40	
ICC	0.11	
N	281	
Observations	51000	
Bayesian R^2	0.40	

Note: Posterior mean and 95% highest density interval (HDI) are reported for all coefficients. Age group 25-55 is the reference level for the categorical variable age group. σ^2 indicates the individual-level variance and τ the variation between individual intercepts and average intercept. ICC is the intraclass correlation coefficient.

Supplementary Model Results

Table S4. Summary of model results over all participants and separated by age group

Group	Model	R^2	n	nLL	pxp	Gener. λ	Error Var. $\sqrt{\theta_\varepsilon^2}$	Explor. β	Temp. τ	Epsi. ε
Overall										
	GP-UCB	0.34	178	483.94	>.99	0.66		0.38	0.03	
	λ lesion	0.18	23	609.91	<.01		4.3	0.3	0.05	
	β lesion	0.24	47	563.62	<.01	1.66			0.13	
	τ lesion	0.2	33	599.93	<.01	0.32		1.94		0.6
Age 5-6										
	GP-UCB	0.11	14	371.15	.60	0.42		0.55	0.07	
	λ lesion	0.02	3	405.8	.07		2.42	12.91	1.03	
	β lesion	0.03	2	401.43	.07	1.43			0.23	
	τ lesion	0.11	11	372.18	.27	0.15		5.23		0.75
Age 7-8										
	GP-UCB	0.26	32	478.06	>.99	0.45		0.52	0.02	
	λ lesion	0.05	0	611.19	<.01		2.79	3.94	0.18	
	β lesion	0.1	4	581.7	<.01	1.57			0.18	
	τ lesion	0.17	11	530.1	<.01	0.15		7.17		0.61
Age 9-10										
	GP-UCB	0.36	24	525.57	>.99	0.67		0.38	0.03	
	λ lesion	0.17	1	682.01	<.01		3.26	0.29	0.07	
	β lesion	0.25	8	614.91	<.01	1.64			0.14	
	τ lesion	0.21	4	650.85	<.01	0.27		2.18		0.6
Age 11-13										
	GP-UCB	0.36	32	533.65	>.99	0.67		0.37	0.03	
	λ lesion	0.17	5	687.85	<.01		4.9	0.28	0.04	
	β lesion	0.26	10	616.47	<.01	1.63			0.12	
	τ lesion	0.19	3	671.15	<.01	0.51		0.54		0.62
Age 14-17										
	GP-UCB	0.4	25	498.37	>.99	0.72		0.34	0.03	
	λ lesion	0.25	5	627.3	<.01		4.25	0.26	0.03	
	β lesion	0.29	9	587.46	<.01	1.72			0.1	
	τ lesion	0.23	3	640.55	<.01	0.95		0.3		0.58
Age 18-24										
	GP-UCB	0.43	32	470.78	>.99	0.89		0.28	0.03	
	λ lesion	0.28	6	595.40	<.01		5.45	0.28	0.01	
	β lesion	0.34	6	550.87	<.01	1.82			0.07	
	τ lesion	0.24	0	634.72	<.01	1.26		0.22		0.53
Age 25-55										
	GP-UCB	0.43	19	471.26	>.99	1.23		0.24	0.03	
	λ lesion	0.29	3	590.8	<.01		3.96	0.24	0.02	
	β lesion	0.36	8	532.53	<.01	2.1			0.07	
	τ lesion	0.22	1	646.14	<.01	1.19		0.21		0.57

Note: We report the average predicted accuracy per model (R^2), the amount of participants best described by the respective model (n), the average out-of-sample negative log likelihood (nLL), the protected exceedance probability (pxp), and median parameter estimates of Generalization λ, Error Variance $\sqrt{\theta_\varepsilon^2}$, Exploration β, Temperature τ, and the epsilon-greedy parameter ε.

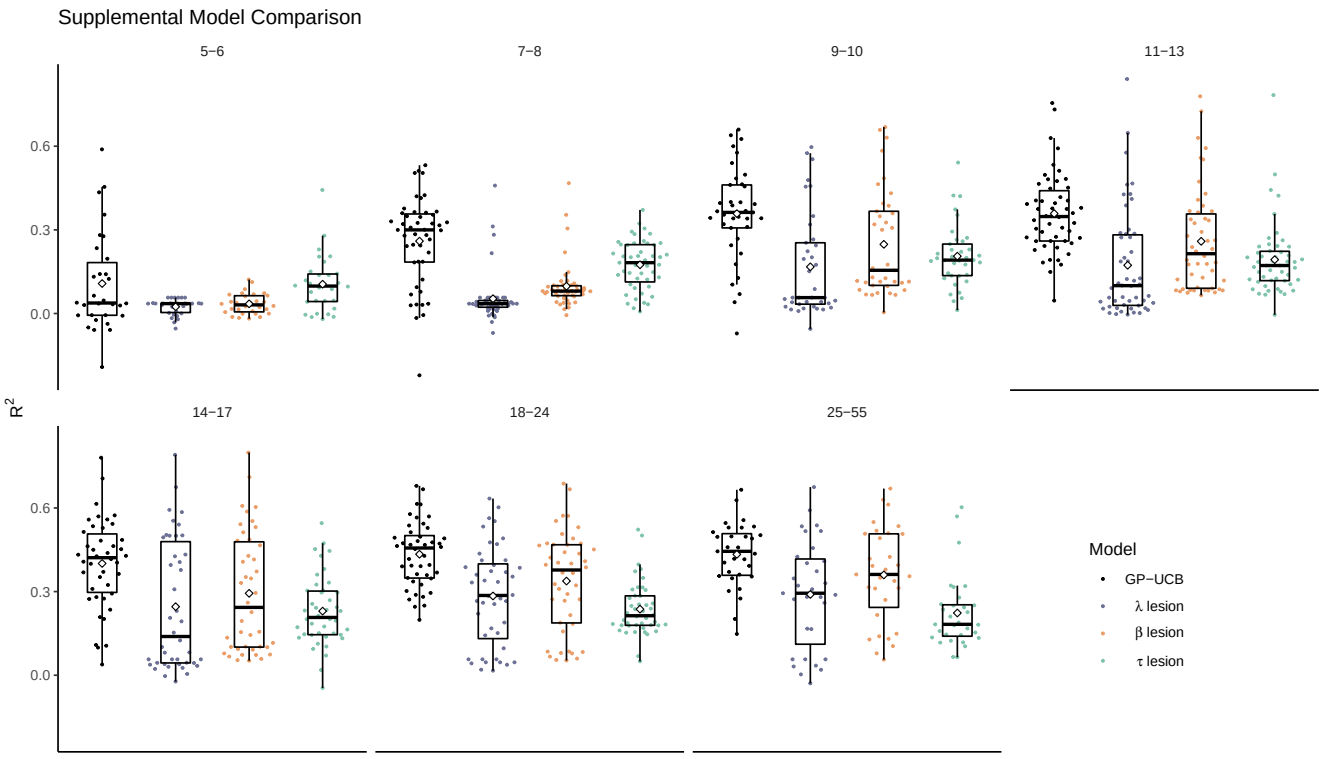

Figure S3. Supplemental model comparisons. Tukey's boxplots showing the predictive accuracy for all models and age groups. Each dot is the predictive accuracy for one participant, white diamonds indicate the group mean.

Model recovery

A prerequisite for interpreting computational models is to ensure each model is uniquely identifiable[85]. To establish that this is the case for models under consideration, we simulated experiments using the subject-level parameter estimates from each model. These simulations were performed using the same set of environments experienced by participants and generated the same data structure as recorded from participants. We then re-estimated each model to the simulated data sets and evaluated how often each model provided the best account of the generated data (based on the summed nLLs over from leave-one-round-out cross-validation). This provides an estimate of the probability with which each model best fits the data given a known simulating model (Figure S4 top row; in each plot, the columns sum to 1). Based on these probabilities we also computed the inverse matrix, using Bayes theorem to define the probability that a model in fact generated the data given that observation that it provided the best fit to the data (Figure S4 bottom row; in each plot, the rows sum to 1).

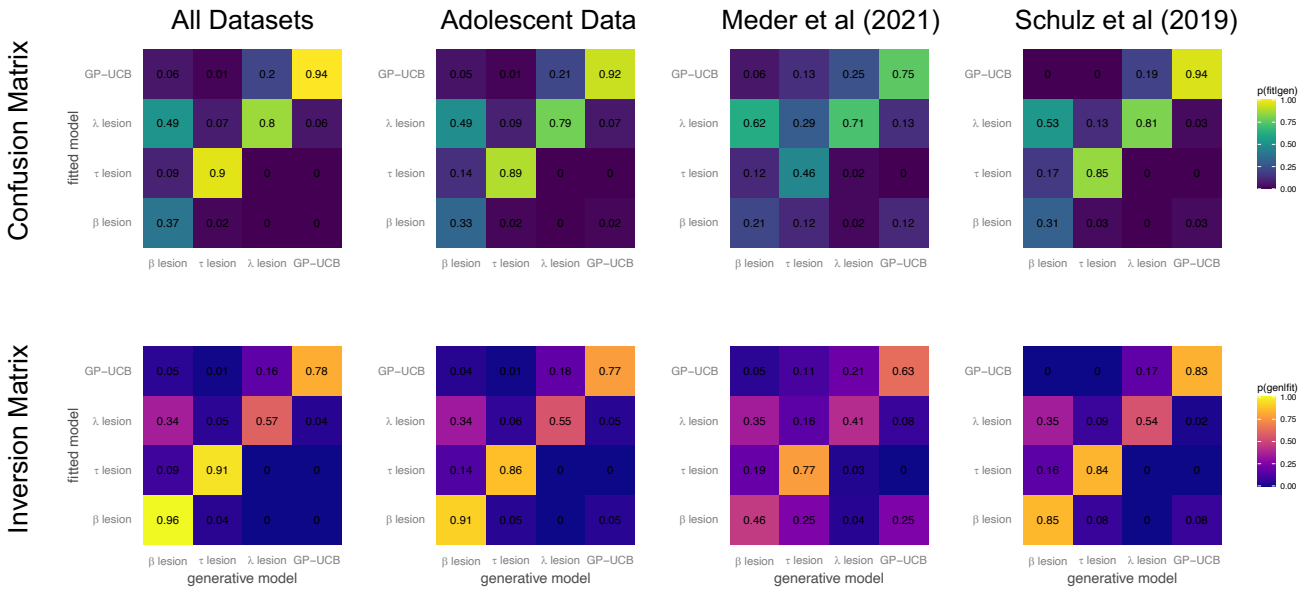

Figure S4. Model Recovery. **Top row**: Confusion matrices showing the probability that a model provides the best out-of-sample predictions (y-axes), given an underlying generative model (x-axes), where behavior was generated using participant parameter estimates. Columns sum to 1 (subject to rounding error). **Bottom row**: Inversion matrices showing the probability that a model did in fact generate the data (x-axes), given that it was found to provide the best out-of-sample predictions (y-axes). Rows sum to 1 (subject to rounding error). The first column refers to all experiments combined, subsequent columns show individual experiments

Parameter recovery

We simulated choices using the winning GP-UCB in order to establish whether the models' parameter estimates are reliable. We evaluated the recoverability of the GP-UCB parameters based on two procedures.

First, following ref[85], we produced a synthetic data-set by simulating choices the base of all empirical subject-level parameter estimates obtained from fitting model to the adolescent data set (Figure S5a; for recovery analyses of the other data-sets see[27]). In all cases, recovered parameters were highly correlated with the parameters used to generate the data (all $r_\tau > .91$, $p < .001$, $BF > 100$).

Second, we performed a more rigorous parameter recovery by iteratively varying each parameter of the GP-UCB model over 20 linearly spaced values within a credible interval of parameter estimates in all experiments (using Tukeys' fence). This creates a set of counter-factual parameters to test whether we can recover parameters we did not originally estimate from the data. Again, we find a high degree of correlation between recovered and generating parameter value (all $r_\tau > .86$, $p < .001$, $BF > 100$).

While the first parameter recovery provides evidence that empirically observed parameter values are recoverable, the second analysis provides additional evidence that even counterfactual parameters (within a credible interval across all datasets) are also recoverable.

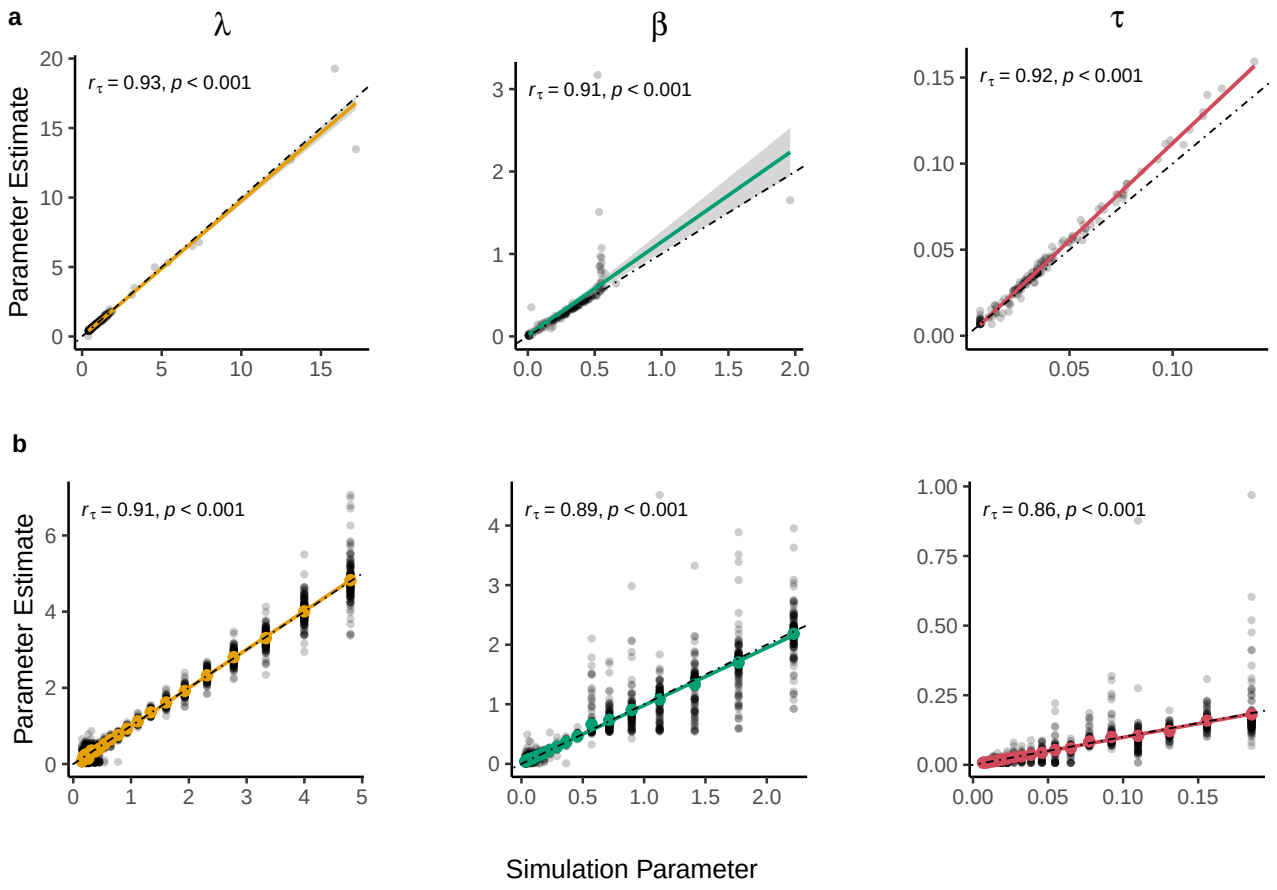

Figure S5. Parameter recovery (GP-UCB). **a**) Parameter recovery using participant parameter estimates to generate data. The black dots denote individual parameter estimates. The colored lines show linear fit, while the dotted line denotes a diagonal indicative of perfect recovery. **b**) Augmented parameter recovery, using participant parameters but with systematic variation across a log-space grid of plausible counterfactual parameter values. This provides additional robustness by simulating data across a wider range of possible parameters. Black dots denote each simulated and generating parameter, while the colored dots the mean 95%CI. The colored lines show linear fit, while the dotted line denotes a perfect recovery. The insetted statistics refer to the rank correlation between generative and fitted parameters, Kendalls τ.

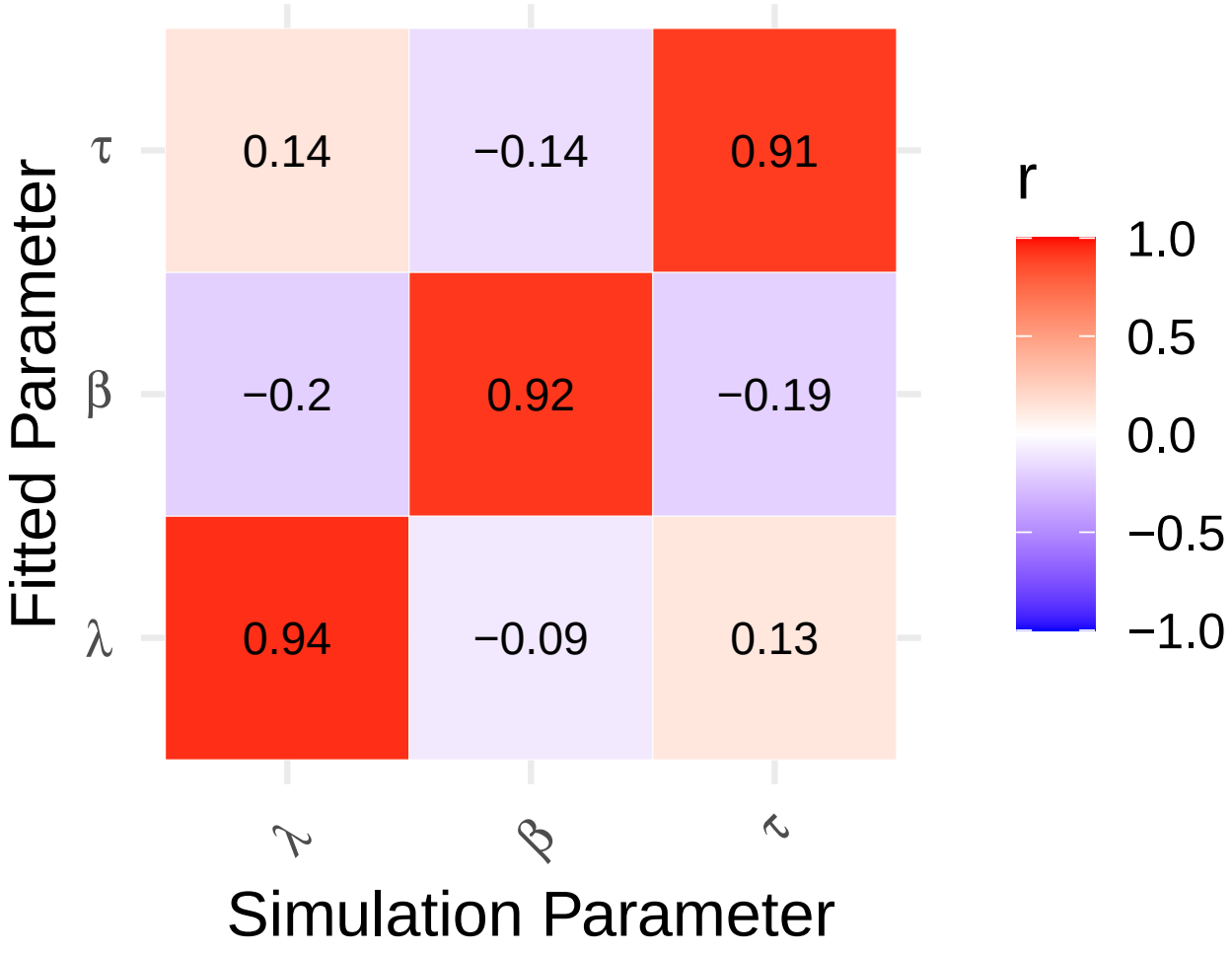

Figure S6. Parameter recovery (GP-UCB). **a**) Estimated parameters correlate strongly with their counterparts used for simulation (diagonal) while correlations with other parameters used for simulation (off-diagonal) are weak.

Comparison of Parameter Regression Models

For all regression models quantifying the relationship between the GP-UCB parameters and age we computed approximate leave-one-out cross validation using pareto-importance sampling as described in Ref[86]. We then used the resulting expected log pointwise predictive densities as model selection criterion. We included models that predicted log-transformed and untransformed parameters. Due to the bounded range of parameter values (> 0), log-transformation resulted in more accurate regression models.

Table S5. Comparison of Parameter Regression Models

Model Class	Transformation	elpd_diff	se_diff	elpd_loo	se_elpd_loo	p_loo	se_p_loo	looic	se_looic
Changepoint	log	0.000000	0.000000	-1300.948	50.48478	33.61886	6.419699	2601.897	100.96956
4th degree polynomial	log	-7.645817	3.898103	-1308.594	49.93090	32.89042	6.255166	2617.188	99.86179
3rd degree polynomial	log	-8.591376	5.105124	-1309.540	50.65230	31.13398	6.143772	2619.079	101.30460
2nd degree polynomial	log	-10.876295	6.552031	-1311.825	51.54652	28.73522	5.991910	2623.649	103.09304
Linear	log	-13.945475	7.652849	-1314.894	52.22692	25.43520	5.634014	2629.788	104.45383
Changepoint	none	-614.963523	147.352916	-1915.912	178.84787	127.23947	63.851037	3831.824	357.69573
4th degree polynomial	none	-616.156643	145.789407	-1917.105	177.06655	120.84630	60.607442	3834.210	354.13309
2nd degree polynomial	none	-616.415606	146.075088	-1917.364	177.57634	120.07705	60.607337	3834.728	355.15269
3rd degree polynomial	none	-618.210471	146.807664	-1919.159	178.14811	127.37190	65.709042	3838.318	356.29623
Linear	none	-620.134252	148.303877	-1921.083	179.86334	119.26099	60.089972	3842.165	359.72667

Note: Comparison of regression models predicting log-transformed parameter estimates as a function of age. Models are described in descending order of fit (best models first). elpd_diff describes the difference in expected log point-wise predictive density, relative to the model with the best predictive accuracy, while se_diff, denotes the standard error of the difference. elpd_loo describes the Bayesian LOO estimate of the expected log pointwise predictive density (Eq 4 in Ref[86]), which is the sum of $n = 281$ pointwise predictive densities, with se_elpd_loo denoting the standard error. p_loo, is the difference between the elpd-loo and the non-cross-validated predictive density, with se_p_loo denoting the standard error. Lastly, looic is the loo information criterion $-2 * \text{elpd}$ and can be interpreted similarly to other information criteria such as BIC or AIC, with se_looic denoting its standard error.

Lesioned Parameter Regression Models

Following the same procedure as above, we also computed approximate leave-one-out-cross-validation of regression models that constrain the changepoints to some parameters, while other parameters were treated as an intercept-only model. To do so, we used the multivariate syntax implemented in brms[87], allowing us to implement any combination of changepoint and intercept-only models for all parameters. The first row denotes the parameter that was fitted using an intercept-only model. The other parameters were fitted as a changepoint model, according to Equation 14.

Table S6. Comparison of Lesioned Parameter Regression Models

Model Class	elpd_diff	se_diff	elpd_loo	se_elpd_loo	p_loo	se_p_loo	looic	se_looic
No intercept only	0.000000	0.000000	-1300.558	50.35418	33.29739	6.355287	2601.117	100.70836
λ intercept only	-3.862616	4.691819	-1304.421	49.35334	29.56012	5.826601	2608.842	98.70668
τ intercept only	-7.336907	6.778480	-1307.895	53.07852	29.10912	5.851021	2615.790	106.15704
β intercept only	-9.909657	6.369223	-1310.468	52.48454	29.38624	6.112272	2620.936	104.96908
λ_β intercept only	-10.228406	6.597255	-1310.787	51.65019	26.63042	5.769139	2621.573	103.30039
λ_τ intercept only	-16.958107	8.738406	-1317.516	52.08509	26.51306	5.760537	2635.033	104.17018
β_τ intercept only	-17.402415	8.865649	-1317.961	53.73732	26.66973	6.113856	2635.921	107.47463

Note: Comparison of regression models predicting log-transformed parameter estimates as a function of age. Models are described in descending order of fit (best models first). elpd_diff describes the difference in expected log point-wise predictive density, relative to the model with the best predictive accuracy, while se_diff, denotes the standard error of the difference. elpd_loo describes the Bayesian LOO estimate of the expected log pointwise predictive density (Eq 4 in Ref[86]), which is the sum of $n = 281$ pointwise predictive densities, with se_elpd_loo denoting the standard error. p_loo, is the difference between the elpd-loo and the non-cross-validated predictive density, with se_p_loo denoting the standard error. Lastly, looic is the loo information criterion $-2 * \text{elpd}$ and can be interpreted similarly to other information criteria such as BIC or AIC, with se_looic denoting its standard error.

Parameter Regression Models

Table S7. Parameters of the changepoint regression models on participant data

Model	Parameter	Estimate	Est.Error	l-95% CI	u-95% CI	Rhat	Bulk_ESS	Tail_ESS
λ (Generalization)								
	Intercept	-0.11	0.12	-0.36	0.12	1	2938	3158
	b1	0.08	0.07	0.02	0.26	1	2288	930
	b2	0.01	0.01	-0.01	0.02	1	4060	5689
	ω	12.70	0.64	7.60	19.80	1	2141	1158
β (Directed Exploration)								
	Intercept	-1.48	0.15	-1.78	-1.19	1	4192	5086
	b1	-0.39	0.17	-0.79	-0.13	1	4252	3638
	b2	0.00	0.01	-0.03	0.02	1	4961	5561
	ω	9.10	0.23	7.44	11.40	1	4087	4767
τ (Random exploration)								
	Intercept	-3.67	0.14	-3.92	-3.42	1	5423	5993
	b1	-0.59	0.20	-1.05	-0.25	1	5266	4086
	b2	0.01	0.01	-0.01	0.03	1	5790	5385
	ω	7.74	0.08	6.88	8.77	1	4513	3495

Note: The models were fit using Hamiltonian Monte-Carlo sampling with 4 Markov chains, each drawing 4000 samples, 2000 of which were discarded as warm-up. The first column (Estimate) refers to the maximum a posteriori estimate of the respective parameters. The second column (Est.Error) denotes the standard deviation of the posterior. The third and fourth column denote the lower and upper credible interval of the posterior. The fifth column denotes the Gelman Rubin Statistic (Rhat) indicating chain convergence. The sixth and seventh columns shows the number of effective samples from the bulk and the tail of the posterior.

Table S8. Parameters of the changepoint regression models on SHC-Fast trajectory

Model	Parameter	Estimate	Est.Error	l-95% CI	u-95% CI	Rhat	Bulk_ESS	Tail_ESS
λ (Generalization)								
	Intercept	0.25	0.02	0.22	0.28	1	1708	1898
	b1	4.84	0.19	4.46	5.23	1	2286	1870
	b2	0.10	0.07	-0.03	0.23	1	1815	1905
	ω	310.35	762.52	294.09	326.21	1	1575	1989
β (Directed Exploration)								
	Intercept	-1.15	0.01	-1.17	-1.13	1	2178	2245
	b1	-2.78	0.35	-3.49	-2.10	1	2019	2106
	b2	0.00	0.04	-0.08	0.08	1	2539	2234
	ω	178.14	787.11	145.89	207.77	1	1250	1623
τ (Random exploration)								
	Intercept	-3.97	0.02	-4.01	-3.93	1	1452	1469
	b1	-3.14	0.31	-3.74	-2.54	1	2029	2385
	b2	0.30	0.07	-0.43	-0.15	1	2066	1957
	ω	255.91	777.67	229.35	293.56	1	1284	1354

Note: The models were fit using Hamiltonian Monte-Carlo sampling with 4 Markov chains, each drawing 4000 samples, 2000 of which were discarded as warm-up. The first column (Estimate) refers to the maximum a posteriori estimate of the respective parameters. The second column (Est.Error) denotes the standard deviation of the posterior. The third and fourth column denote the lower and upper credible interval of the posterior. The fifth column denotes the Gelman Rubin Statistic (Rhat) indicating chain convergence. The sixth and seventh columns shows the number of effective samples from the bulk and the tail of the posterior.

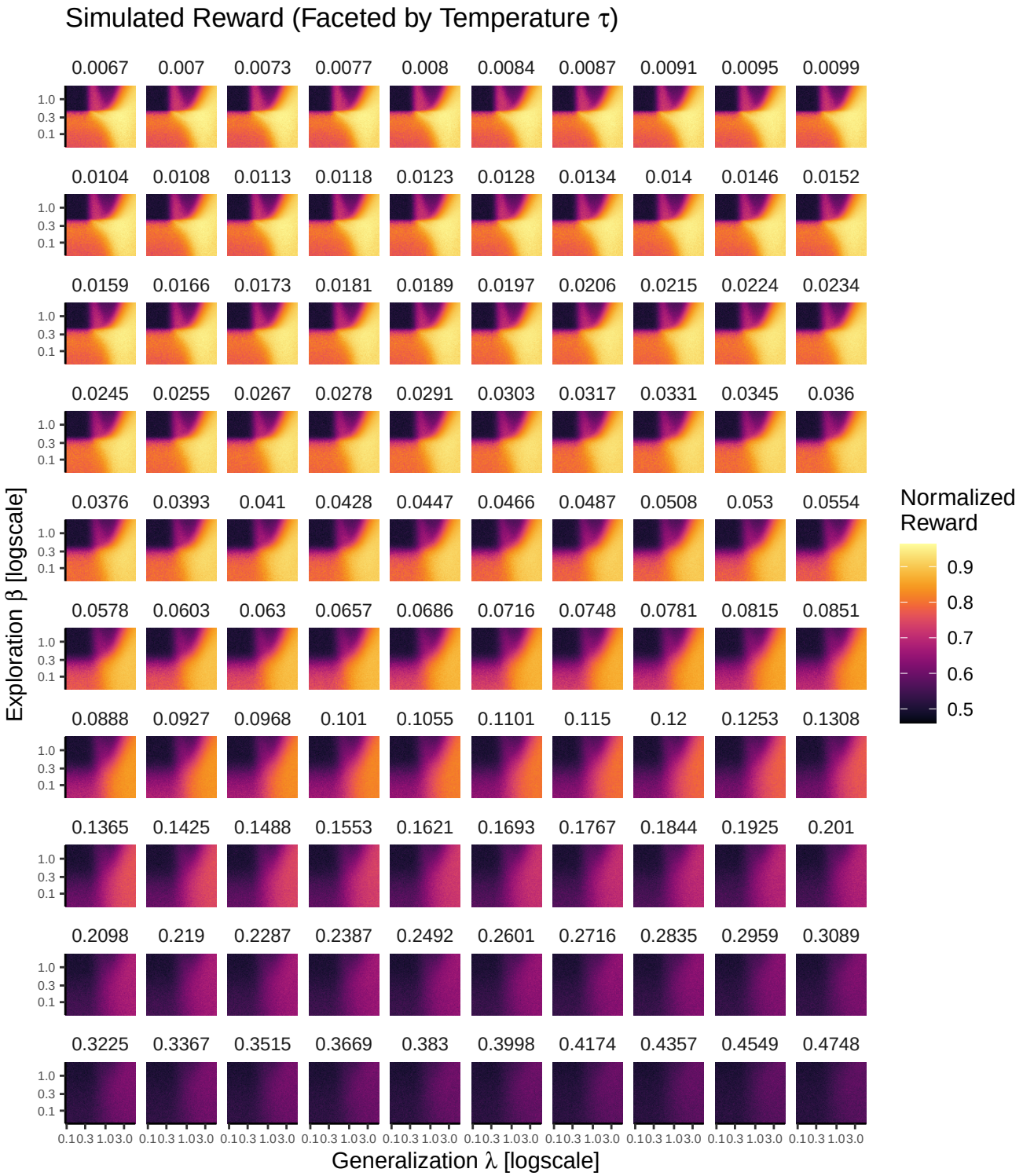

Figure S7. Fitness landscape. The 3-dimensional fitness landscape is computed over 1 million parameter combinations across λ (x-axis), β (y-axis), and τ (facets). For each parameter, we defined 100 equally log-spaced values over a credible range of participant parameter estimates (using Tukey's fence). We then simulated 100 rounds of the task using each combination of parameters (sampling with replacement from the same set of 40 environments given to participants) in order to compute an average reward, which we then normalized to a max of 1.

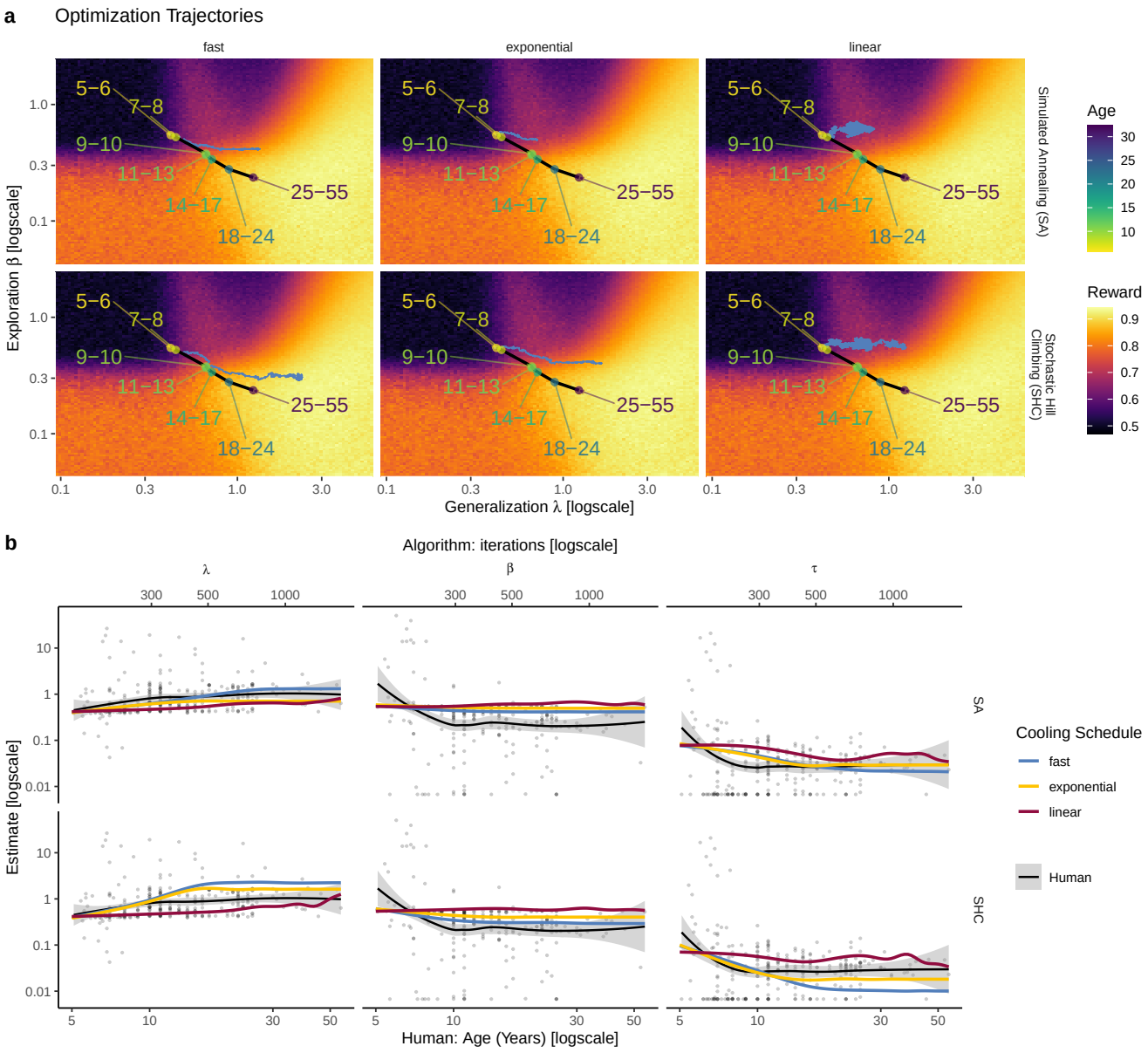

Figure S8. Supplementary results of the optimization algorithms. **a**) Trajectories of λ and β for each combination of optimization algorithm (rows) and cooling function (columns). For the background, we used the τ value with the smallest difference to the mean simulated τ value across all trajectories and iterations ($\bar{\tau} = .03$). Human estimates (labeled dots) are also provided for comparison. **b**) Comparison of the human developmental trajectory (black line indicates smoothed means ± 95% CI and dots show each individual parameter) to each optimization algorithm (colored lines). Human data is plotted along age in years (bottom axis), while the algorithm results are plotted in terms of iteration number (top axis), both in log scale.

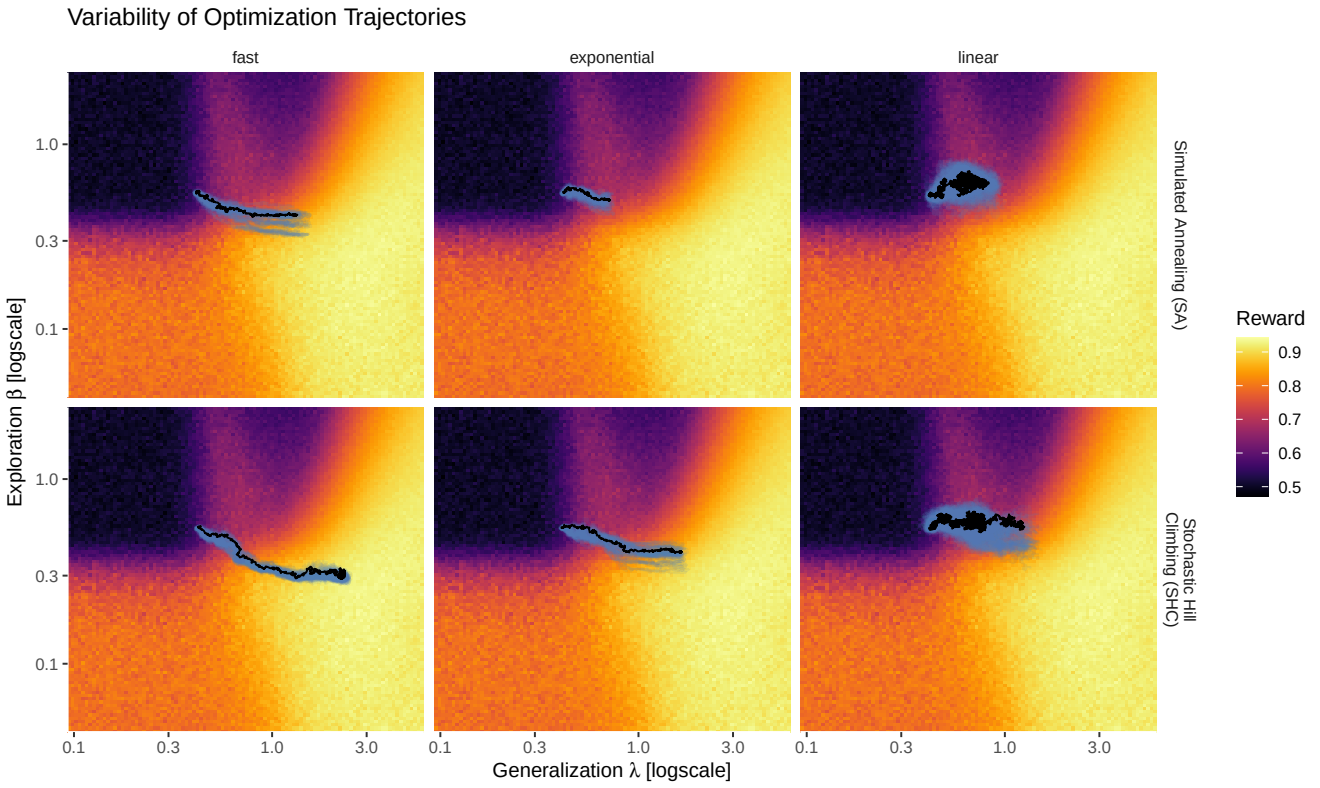

Figure S9. Variability of trajectories of generalization λ and uncertainty-directed exploration β. Plots show the bootstrapped variability of trajectories (blue) as well as the median trajectories (black) for each combination of optimization algorithm (rows) and cooling function (columns). Each combination of algorithm and cooling schedule was initialized with all individual cross-validated parameter estimates of the youngest age group once (30 participants $\times$ 4 rounds), which provides us with four trajectories per participant and algorithm. To visualize the variability of algorithm trajectories, we iteratively dropped one of the trajectories for each participant and then use the same aggregation method (mean for each participant and then the median trajectory across participants; 100 iterations). We then plot each of these leave-one-out aggregated trajectories to visualize the variability of the algorithm trajectories.

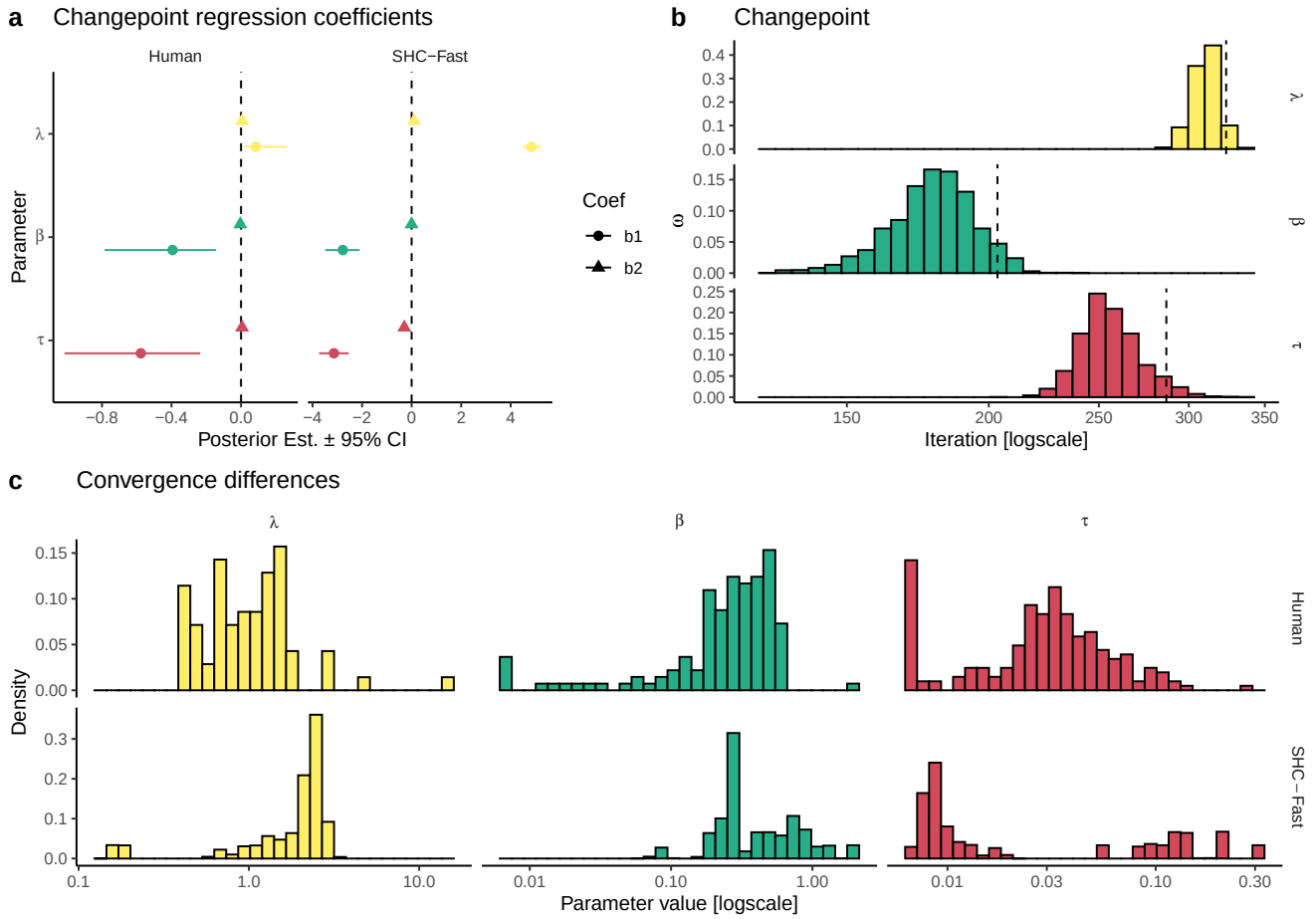

Figure S10. Similarity between human and optimization algorithm. To compute how human and algorithm trajectories differ, we first generated 100 bootstrapped datasets of the SHC-fast cooling trajectories, matched in size to our participant data ($n = 281$). This allows us to run a comparable version of the changepoint regression, comparing humans to the algorithm. Specifically, we first created a unified time variable for human and algorithm trajectories by normalizing participant age and algorithm iterations to the same range of $[0, 1]$, respectively. Then for each (unnormalized) age bin in years [5,6, …, 55], we randomly sampled (without replacement) the same number of parameters (λ, β, τ) from the algorithm trajectory within the same unified time range. This created a matched dataset of the algorithmic trajectory with the same number of $n = 281$ observations along the same unified time axis. This was repeated 100 times to minimize sampling bias. We than re-ran the change-point regression on this bootstrapped data, using the same formulation as in Eq. 14-15. This allows us to compare b_1 and b_2 between humans and the algorithm trajectories, which yielded qualitatively similar trends (see Table S8). **a**) The posterior regression weights of the changepoint regression estimated on both human (left) and algorithm trajectories (SHC-Fast cooling; right). The point-ranges denote the 95% credible interval (CI), while the vertical dashed line indicates 0 (i.e., no change). **b**) Posterior estimates of the changepoint ω from the algorithm trajectories. The vertical dashed line indicates the upper 95% CI. **c**) Parameter distributions after the changepoint (thresholded at the upper 95% CI of the respective ω estimates). The upper panel shows human parameters and the lower panel shows parameters sampled by the SHC algorithm with fast cooling. Human λ and β parameters converged at lower values than the algorithm (λ: $U = 2740$, $p < .001$, $r_\tau = -.38$, $BF > 100$; β: $U = 10114$, $p < .001$, $r_\tau = -.19$, $BF > 100$), while τ estimates were not reliably higher or lower ($U = 22377$, $p = .188$, $r_\tau = .05$, $BF = .12$).